nature communications

Article

https://doi.org/10.1038/s41467-024-54093-5

Human Disabled-2 regulates thromboxane A_2 signaling for efficient hemostasis in thrombocytopenia

Received: 24 April 2023

Accepted: 30 October 2024

Published online: 13 November 2024

Check for updates

Hui-Ju Tsai[1], Ya-Fang Chang[1], Ya-Ju Hsieh[2], Jiaan-Der Wang[3,4], Chih-Ching Wu[1,2,5,6], Meng-Ying Ho[1], Ju-Chien Cheng[7], Ding-Ping Chen[1,8], Hsiang-Rui Liao[6,9,10] & Ching-Ping Tseng[1,6,8]

Understanding platelet protein functions facilitates better assessment of platelet disorders. Megakaryocyte lineage-restricted human Disabled-2 knock-in (*hDAB2-KI*) mice are generated to delineate the functions of hDab2, a regulator of platelet function, in the control of bleeding associated with thrombocytopenia. Here we show that *hDab2-KI* mice with thrombocytopenia display decreased bleeding time when compared to the control mice. hDab2 augments thromboxane A_2 (TxA_2) mimetic U46619- but not other agonists-stimulated granule secretion, integrin activation, and aggregation at a lower platelet concentration in vitro. Binding of hDab2 to phosphatidic acid (PA) facilitates formation of the PA-hDab2-AKT complex leading to an increase in U46619-stimulated AKT-Ser473 phosphorylation and the first wave of ADP/ATP release. Consistent with these findings, hDab2 expression in platelets from patients with immune thrombocytopenic purpura is positively correlated with U46619-stimulated ATP release, which in turn inversely correlated with their bleeding tendency. hDab2 appears crucial in regulating bleeding severity associated with thrombocytopenia by a functional interplay with ADP/ATP release underlying TxA_2 signaling.

Hemostasis is a process to stop bleeding when blood vessels are damaged. At injured sites, platelets are activated by the subendothelial matrix and plasma proteins such as collagen and von Willebrand factor leading to thrombin generation[1,2]. Platelet activation is further amplified by the release of thromboxane A_2 (TxA_2) and ADP[3,4]. A balance of platelet activation and platelet number is important for maintenance of normal hemostasis. Hyperactive platelets or an increase in the platelet count leads to thrombotic disorders such as stroke or myocardial disease, while hypoactive platelets or a decrease in the platelet count leads to bleeding when vascular integrity is disrupted[5–8]. Thrombocytopenia is a disorder associated with an increased bleeding tendency. The bleeding severity of patients with thrombocytopenia is closely related to the platelet count and functions[9–11]. Understanding how platelets are

[1]Department of Medical Biotechnology and Laboratory Science, College of Medicine, Chang Gung University, Taoyuan 333, Taiwan, Republic of China. [2]Molecular Medicine Research Center, Chang Gung University, Taoyuan 333, Taiwan, Republic of China. [3]Children's Medical Center, Taichung Veterans General Hospital, Taichung 407, Taiwan, Republic of China. [4]Department of Post-Baccalaureate Medicine, College of Medicine, National Chung Hsing University, Taichung 402, Taiwan, Republic of China. [5]Department of Otolaryngology-Head and Neck Surgery, Chang Gung Memorial Hospital, Taoyuan 333, Taiwan, Republic of China. [6]Graduate Institute of Biomedical Sciences, College of Medicine, Chang Gung University, Taoyuan 333, Taiwan, Republic of China. [7]Department of Medical Laboratory Science and Biotechnology, China Medical University, North District, Taichung 404, Taiwan, Republic of China. [8]Department of Laboratory Medicine, Chang Gung Memorial Hospital, Taoyuan 333, Taiwan, Republic of China. [9]Graduate Institute of Natural Products, College of Medicine, Chang Gung University, Taoyuan 333, Taiwan, Republic of China. [10]Department of Anesthesiology, Chang Gung Memorial Hospital, Taoyuan 333, Taiwan, Republic of China. e-mail: ctseng@mail.cgu.edu.tw

activated is important for developing therapeutic agents and the new tools to predict bleeding status.

Patients with a higher bleeding tendency have lower levels of platelet surface activated integrin αIIbβ3 and P-selectin following agonist stimulation[10], indicating that proteins involved in platelet activation are key factors for determining bleeding risk. However, there are still patients with thrombocytopenia whose bleeding risk cannot be simply explained by the current prediction models[11]. Platelet protein functions in thrombocytopenia are warranted to investigate further. Among the platelet proteins, Disabled-2 (Dab2) is a multifunctional adaptor protein and is a key regulator of platelet activation[12–16]. There are at least two alternative splicing isoforms p82 and p59[17]. p82 is the full-length isoform while p59 lacks the ninth coding exon corresponding to the amino acids 230 to 447 of p82, resulting in the deletion of several binding sites for endocytic proteins[17,18]. The two Dab2 isoforms elicit different functional activities within cells. p59 but not p82 acts as a transcriptional activator during the differentiation of murine F9 embryonal carcinoma cells[19]. p82 entirely rescues endocytosis in the visceral endoderm of E6.5 embryos while p59 lacks some endocytic protein binding sites and only partly rescues endocytosis[18].

Dab2 is required for efficient hemostasis and platelet activation as revealed in megakaryocyte lineage-restricted *DAB2* knockout mice generated by cross-breeding *DAB2*$^{fl/fl}$ mice with *PF4-Cre* mice to ablate exon 2 of *DAB2* gene[14]. The major Dab2 isoform is different in human and mouse platelets. p59 is the sole Dab2 isoform in mouse platelets while human platelets express the p82 isoform[14]. Dab2 expression is relatively more abundant in humans than in mouse[20]. The role of p82 human Dab2 (hDab2) in platelets is mainly demonstrated by in vitro assays using recombinant proteins or peptides. hDab2 released from α-granules binds either integrin αIIb or the phospholipid sulfatide in response to platelet activation, thereby playing a role in platelet-fibrinogen and platelet-leukocyte adhesion and aggregation[12,13,21–23]. The in vivo functions of hDab2 in hemostasis, thrombus formation, and platelet activation remain to be elucidated.

In this study, megakaryocyte lineage-restricted *hDAB2* knock-in (*hDAB2-KI*) mice were generated by establishing a mouse strain (*Rosa26*$^{fl/fl}$ mice) with site-specific insertion of a conditional hDab2 expression cassette into the *Rosa26* locus followed by cross-breeding the mice with *PF4-Cre* mice. The in vivo activities of platelet hDab2 in hemostasis, thrombus formation, and platelet function were then determined. We revealed that p82 hDab2 enhanced TxA_2 signaling and subsequent ADP release leading to reduced bleeding under thrombocytopenic conditions. This was also supported by the findings in patients with immune thrombocytopenic purpura (ITP).

Results

Generation of megakaryocyte lineage-restricted *hDAB2-KI* mice

Insertion of a gene in the *Rosa26* locus permits consistent gene expression[24,25]. *Rosa26*$^{fl/fl}$ mice with a conditional *hDAB2* gene expression cassette inserted into the *Rosa26* locus were developed in order to generate the megakaryocyte lineage-restricted *hDAB2-KI* mice. The conditional *hDAB2* gene expression cassette which contained a CAG promoter, a stop cassette (PGK-*Neo*-4XpA) flanked by two *LoxP* sites, and hemagglutinin-tag *hDAB2* sequences (*HA-hDAB2*) was flanked by *Rosa26* genomic sequences. The stop cassette was composed of the PGK promoter driving neomycin resistance gene (*Neo*) expression and four polyadenylation (4XpA) sequences. The suicide gene encoding catalytic diphtheria toxin fragment A (*DTA*) was placed downstream of the *Rosa26* locus (Fig. 1a). The pRosa26PA-c-hDAB2-KI plasmid was transfected into the *JM8A* embryonic stem cells (ESCs) followed by positive and negative selection with G418 and diphtheria toxin, respectively. ESCs that underwent homologous recombination and carried the conditional *hDAB2* gene expression cassette (fl allele) were characterized by Southern blot analysis of EcoRV-digested genomic DNA using a S1 probe (536 bps). The appearance of 11.5 kb and 6 kb band indicated the presence of a wild-type *Rosa26* allele (+) and a fl allele in the genome of ESCs, respectively (Fig. 1a, b). The ESCs containing a fl allele were injected into early embryos from *C57BL/6* mice and implanted into pseudo-pregnant *ICR* mice to generate the *Rosa26*$^{fl/+}$ mice which were then interbred to obtain *Rosa26*$^{fl/fl}$ mice. Megakaryocyte lineage-restricted *hDAB2-KI* mice were generated by cross-breeding *Rosa26*$^{fl/fl}$ mice with *PF4-Cre* mice[26] (Fig. 1c). Genotyping of newborn pups tail genomic DNA by PCR revealed the PCR products of 447, 320, and 450 bps corresponding to the wild-type *Rosa26* allele (+), fl allele, and *PF4-Cre* gene (Cre), respectively (Fig. 1a, c, d). HA-hDab2 protein (p82) was detectable in *hDAB2-KI* but not *Rosa26*$^{fl/fl}$ platelets (Fig. 1e). Dab2 expression was comparable in lung, liver, kidney, spleen and intestine between *Rosa26*$^{fl/fl}$ and *hDAB2-KI* mice (Supplementary Fig. 1). These data confirm the generation of megakaryocyte/platelet-restricted *hDAB2-KI* mice.

hDAB2-KI mice display normal appearance, platelet biogenesis, hemostasis and thrombus formation, but a reduced bleeding time in mice with thrombocytopenia

The appearance, platelet morphology, number of α- and δ-granules, ADP and ATP content, bleeding time, rebleeding rate (Fig. 2a–f), and complete blood count (Supplementary Table 1) of *hDAB2-KI* mice were comparable to the *Rosa26*$^{fl/fl}$ mice. In the $FeCl_3$-induced mesenteric thrombus formation model, the occlusion time of arterioles and venules was not significantly different between *Rosa26*$^{fl/fl}$ and *hDAB2-KI* mice (Fig. 2g, h and Supplementary Video 1). These data indicate that *hDAB2-KI* mice display normal appearance, platelet biogenesis, hemostasis and thrombus formation.

Peritoneal injection of anti-CD41 antibody (anti-CD41) causes the development of ITP[27]. A prolonged bleeding time was observed when platelet counts were ≤ 5×10^8/ml or approximately 28.8% of the normal count[28]. The *Rosa26*$^{fl/fl}$ and *hDAB2-KI* mice had comparable platelet numbers after injection of anti-CD41 (Fig. 3a). Of the mice with ITP (platelet counts ≤ 5×10^8/ml), 72% and 25% of the *Rosa26*$^{fl/fl}$ and *hDAB2-KI* mice continued to bleed for more than 10 min (Fig. 3a). hDab2 expression in platelets reduced the bleeding time of the mice with ITP (Fig. 3b, $p = 0.0054$). At 72 h after final injection of anti-CD41, platelet counts of both *Rosa26*$^{fl/fl}$ and *hDAB2-KI* mice were recovered to the range between 5.2×10^8/ml and 13×10^8/ml (Fig. 3a). At the recovery phase (RP), 35% and 7.7% of the *Rosa26*$^{fl/fl}$ and *hDAB2-KI* mice continued to bleed for more than 10 min (Fig. 3a). The bleeding time was slightly but not significantly different between *Rosa26*$^{fl/fl}$ and *hDAB2-KI* mice (Fig. 3b, $p = 0.0981$). These data indicate that the effect of platelet hDab2 expression on reducing bleeding is related to the status of thrombocytopenia and the platelet count in mice.

hDab2 selectively augments U46619-stimulated platelet activation at a lower platelet concentration of 1.8×10^8/ml in vitro

Rosa26$^{fl/fl}$ and *hDAB2-KI* platelets displayed similar collagen adhesion activity (Fig. 4a). The aggregation traces of *Rosa26*$^{fl/fl}$ and *hDAB2-KI* platelets in response to low and high concentrations of collagen, thrombin, PAR4 peptide (AYPGKF), and ADP were comparable at a platelet concentration that is routinely used in aggregation studies (2.4×10^8/ml) or at a lower platelet concentration (1.8×10^8/ml) (Fig. 4b). No aggregation was observed with low concentrations of agonists when the platelet concentration was lower than 1.8×10^8/ml (Supplementary Fig. 2). *hDAB2-KI* platelets, when compared to the *Rosa26*$^{fl/fl}$ platelets, displayed an enhanced aggregation response to high concentration of TxA_2 mimetic U46619 (0.5 μM) at a platelet concentration of 1.8×10^8/ml, but not 2.4×10^8/ml. The difference was more prominent when platelets were stimulated by low concentration of U46619 (0.25 μM) (Fig. 3b). Under the same assay conditions, *hDAB2-KI* platelets displayed enhanced U46619-stimulated platelet integrin activation when compared to the *Rosa26*$^{fl/fl}$ platelets as

https://doi.org/10.1038/s41467-024-54093-5

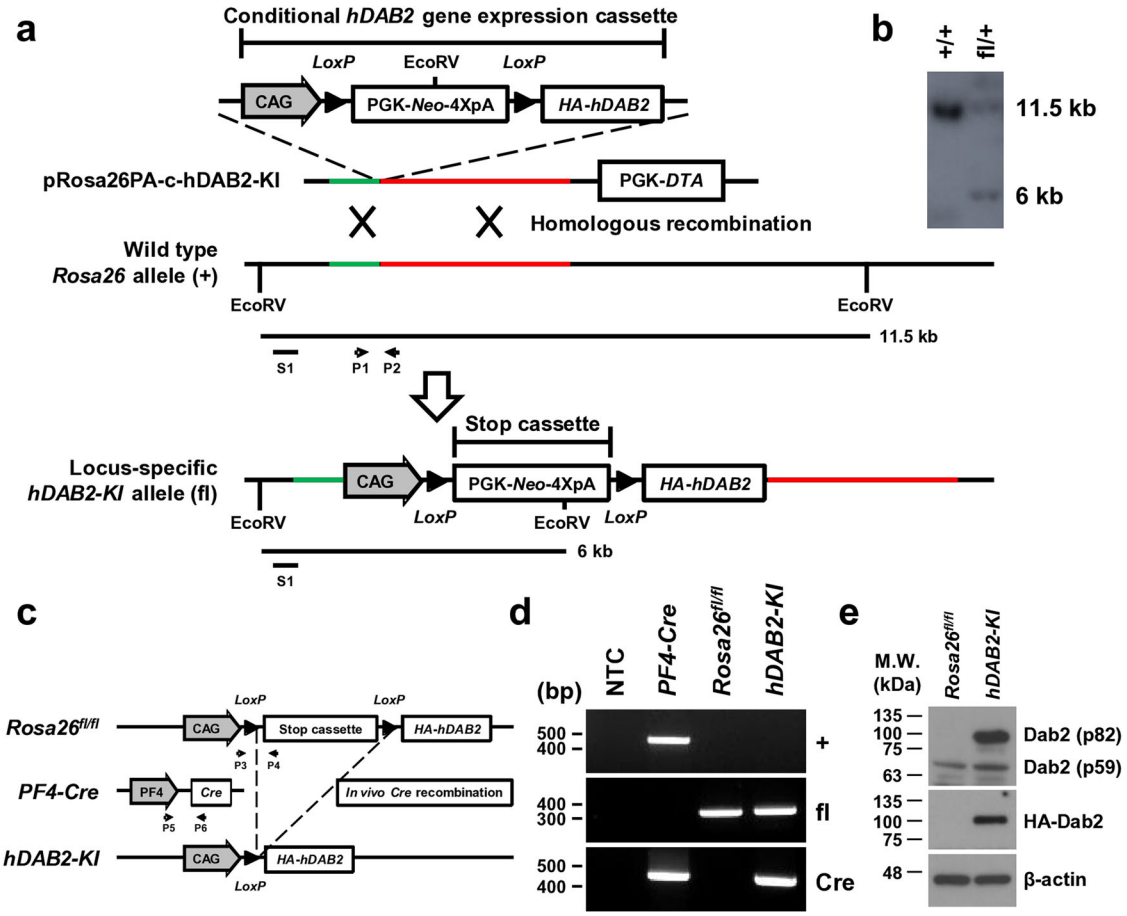

Fig. 1 | Generation of megakaryocyte lineage-restricted *hDAB2-KI* mice. **a** Targeting the conditional *hDAB2* gene expression cassette into the *Rosa26* locus of ESCs. The pRosa26PA-c-hDAB2-KI plasmid containing the conditional *hDAB2* gene expression cassette flanked with *Rosa26* genomic sequences (green and red lines) was transfected into ESCs. Insertion of the expression cassette into the wild-type *Rosa26* locus was obtained by homologous recombination after positive and negative selection with neomycin and diphtheria toxin, respectively. Stop cassette flanked by two *LoxP* sites containing the sequences of PGK promoter, neomycin resistant gene (*Neo*), and 4X polyadenylation signal (4XpA) prevented constitutive *HA-hDAB2* gene expression. *DTA*, diphtheria toxin fragment A. **b** Representative data for the wild-type (+, 11.5 kb) and fl (6 kb) allele are shown. Genomic DNA from 96 ESCs were analyzed by Southern blot. There were 84 ESCs with wild-type (+/+) and 12 ESCs with heterozygous (fl/+) *Rosa26* locus containing one wild-type allele and one allele with the conditional *hDAB2* gene expression cassette. EcoRV-digested genomic DNA was hybridized with a S1 probe as shown in panel **a** for genotyping. **c** Illustration of the genomic positions related to the generation of *Rosa26*$^{fl/fl}$, *PF4-Cre*, and *hDAB2-KI* mice. *hDAB2-KI* mice were generated when the stop cassette was removed by in vivo *Cre-LoxP* recombination through mating *Rosa26*$^{fl/fl}$ mice with *PF4-Cre* mice. **d** Tail genomic DNA from the representative mice were analyzed by PCR for genotyping. Genotyping was performed in over ten independent experiments. The positions of the six PCR primers (P1, P2, P3, P4, P5 and P6) used in the study are indicated in panels **a** and **c**. The PCR products of 447, 320, and 450 bps correspond to the wild-type *Rosa26* allele (+), the locus-specific *hDAB2-KI* allele (fl), and the *PF4-Cre* gene (Cre), respectively. NTC, no template control. **e** The lysates of *Rosa26*$^{fl/fl}$ and *hDAB2-KI* platelets were analyzed by Western blot using antibodies against Dab2, HA-tag, and β-actin, respectively. Representative data from 3 biological replicates are shown. Source data are provided as a Source Data file.

measured by the binding of Alexa Fluor 488-conjugated fibrinogen (Fig. 4c and Supplementary Fig. 3). hDab2 thereby selectively augments TxA_2-stimulated platelet aggregation when the platelet concentration falls below a certain threshold.

hDab2 regulates TxA_2 signaling leading to a reduced bleeding time of *hDAB2-KI* mice with thrombocytopenia

Rosa26$^{fl/fl}$ and *hDAB2-KI* mice were administered low-dose aspirin (25 mg/kg) for 7 days to delineate whether TxA_2 contributes to the reduced bleeding time of *hDAB2-KI* mice with thrombocytopenia. Low-dose aspirin inhibited TxA_2 generation in mice as revealed by the reduced serum concentration of TxB_2 (a stable TxA2 metabolite) which reflects the maximal biosynthetic capacity of blood platelets to generate TxA_2 in response to endogenously formed thrombin during whole-blood clotting (Fig. 5a). The bleeding time for *Rosa26*$^{fl/fl}$ and *hDAB2-KI* mice without injection of anti-CD41 antibody was comparable regardless whether or not the mice were administered aspirin (Fig. 5b). In the absence of aspirin, *hDAB2-KI* mice injected with the anti-CD41 antibody displayed thrombocytopenia with a reduced bleeding time when compared to the *Rosa26*$^{fl/fl}$ mice. Aspirin administration prolonged the bleeding time of *hDAB2-KI* mice with thrombocytopenia (Fig. 5b, c, $p = 0.012$). TxA_2 is thereby crucial for the reduced bleeding time of *hDAB2-KI* mice with thrombocytopenia.

Serum TxB_2 is an ex vivo index of the maximal capacity of platelets to generate TxA_2 in response to thrombin (generated endogenously) strictly dependent on the number of platelets[29]. We found a decrease of serum TxB_2 generation in *Rosa26*$^{fl/fl}$ and *hDAB2-KI* mice injected with anti-CD41 antibody compared to mice injected with the vehicle control ($p < 0.001$) (Fig. 5d). These results reflect the decreased number of platelets in the mice injected with anti-CD41 antibody. Further analysis revealed that *Rosa26*$^{fl/fl}$ and *hDAB2-KI* mice had comparable urinary levels of 2,3-dinor-TxB_2 (a metabolite and an index of TxA_2 generation from platelets in vivo) and 2,3-dinor-6-keto-$PGF_{1\alpha}$ (a metabolite and an index of PGI_2 biosynthesis from vascular cells in vivo) with or without

https://doi.org/10.1038/s41467-024-54093-5

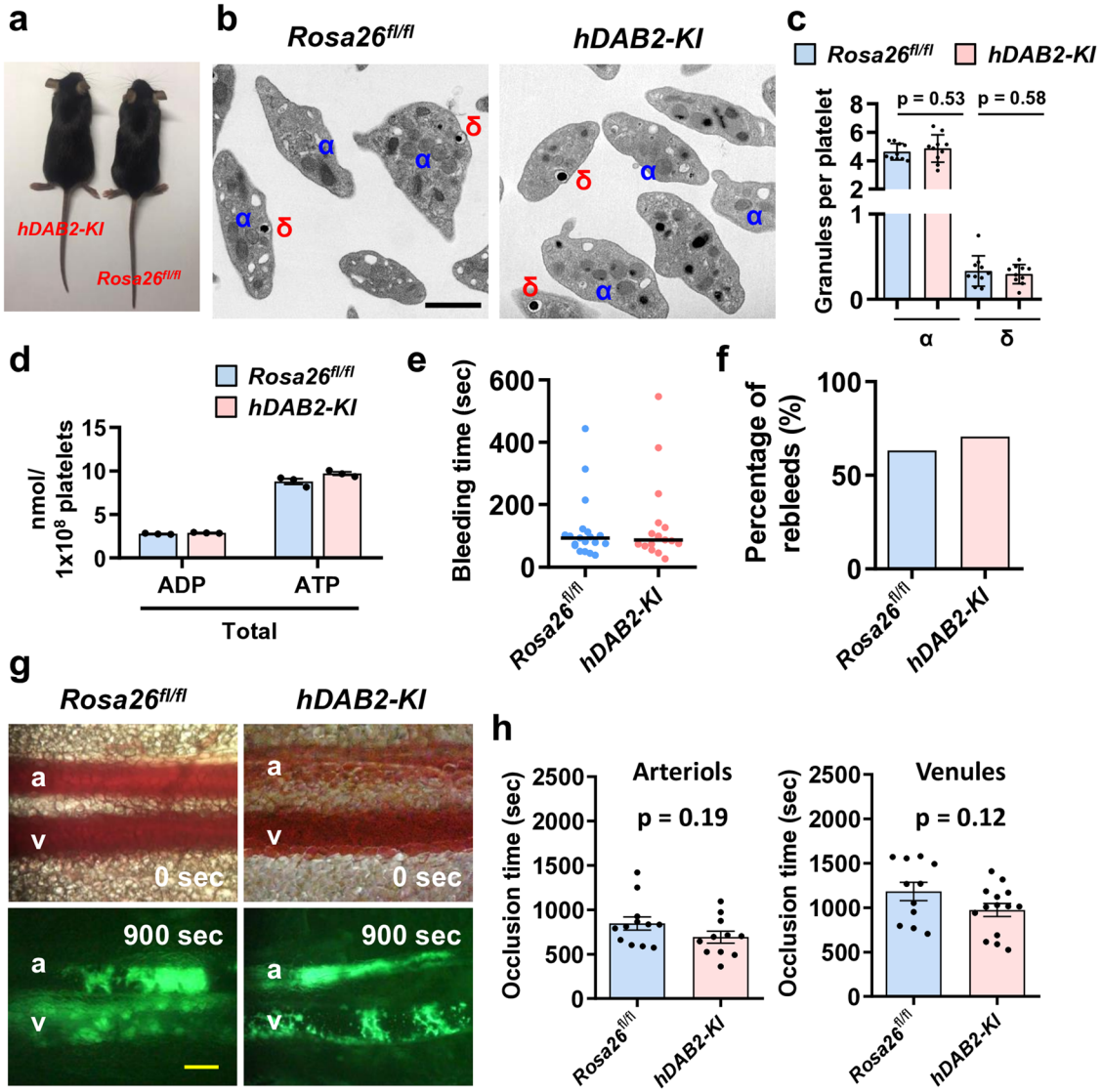

Fig. 2 | *hDAB2-KI* mice display normal appearance, platelet biogenesis, hemostasis and thrombus formation. a The appearance for *Rosa26*$^{fl/fl}$ and *hDAB2-KI* mice. **b, c** Representative TEM images (32,000 X) of platelets from *Rosa26*$^{fl/fl}$ and *hDAB2-KI* mice ($n = 3$ mice per genotype), with quantification of the number of α- and δ-granules per platelet shown in panel c. A total of 144 platelets from *Rosa26*$^{fl/fl}$ mice and 142 platelets from *hDAB2-KI* mice was present in the 10 random fields selected for quantification ($n = 10$). Each data point represents the average number of α- and δ-granules per platelet obtained from one random field. The experiments were repeated two times independently with similar results. α, α-granule; δ, δ-granule. Scale bar = 1 μm. **d** The content of ADP and ATP of washed platelets was analyzed and quantified using the GloMax 20/20 luminometer. Data represent the mean ± SEM of 3 biological replicates each consisting of 3 technical replicates. **e** Bleeding time for the *Rosa26*$^{fl/fl}$ ($n = 19$) and *hDAB2-KI* ($n = 17$) mice was plotted and the horizontal lines represent the median of tail bleeding time. Unpaired two-sided Student's *t*-test was used for statistical analysis of the data in panels (**c**–**e**). $p < 0.05$ was considered statistically significant. Exact *p* values for each group and Source data are provided as a Source Data file. **f** The percentages of mice as described in **e** that were rebled within 2 min after blood flow stop are shown. **g, h** Representative images for *Rosa26*$^{fl/fl}$ ($n = 12$) and *hDAB2-KI* ($n = 16$) mice at 0 and 900 sec following $FeCl_3$ treatment are shown. a, arterioles; v, venules. Scale bar = 200 μm. The occlusion time of the *Rosa26*$^{fl/fl}$ ($n = 12$ for arterioles and $n = 11$ for venules) and *hDAB2-KI* mice ($n = 11$ for arterioles and $n = 14$ for venules) was recorded and analyzed by the two-sided Mann-Whitney U test. $p < 0.05$ was considered statistically significant. Data represent the mean ± SEM. Source data are provided in Source Data file.

injection of anti-CD41 antibody (Fig. 5e). Injection of anti-CD41 antibody caused a slight but not significant increase in urinary 2,3-dinor-TxB_2 for both *Rosa26*$^{fl/fl}$ and *hDAB2-KI* mice. This indicates that in vivo TxA_2 generation and the vascular response of endothelial cells to platelet activation are not affected by hDab2 expression in platelets. The expression of TxA_2 receptor TP at the resting stage (Fig. 5f and Supplementary Fig. 4) and in vitro TxB_2 generation for washed platelets in response to PAR4 peptide or collagen (Fig. 5g) were comparable between *Rosa26*$^{fl/fl}$ and *hDAB2-KI* platelets. These data indicate that hDab2 regulates intracellular signaling downstream of TxA_2 receptor but not in vivo TxA_2 generation.

Augmentation of TxA_2-stimulated ADP/ATP release by hDab2 reduces the bleeding risk of mouse and human with thrombocytopenia

hDAB2-KI platelets displayed an enhanced U46619-stimulated α-granule secretion and δ-granule secretion at a lower platelet concentration of 1.8×10^8/ml when compared to the *Rosa26*$^{fl/fl}$ platelets as measured by the surface expression of CD62P and the release of ADP/ATP, respectively (Fig. 6a and Supplementary Fig. 5). U46619-stimulated aggregation of hDab2-KI platelets at 1.8×10^8/ml was inhibited by apyrase (an ADP/ATP hydrolase) in a dose-dependent manner, while U46619-stimulated *Rosa26*$^{fl/fl}$ and *hDAB2-KI* platelet aggregation was

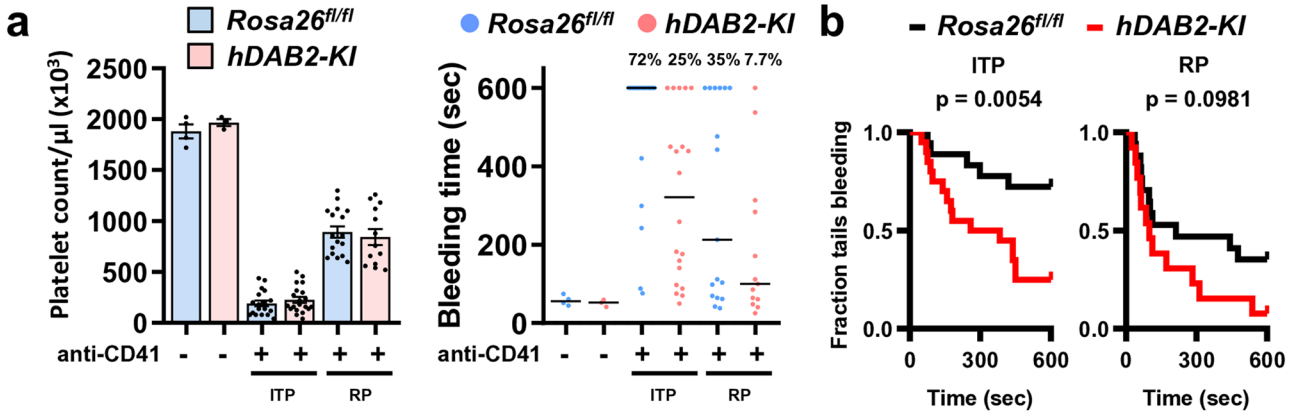

Fig. 3 | *hDAB2-KI* mice with thrombocytopenia display a reduced bleeding time. **a, b** *Rosa26*$^{fl/fl}$ ($n = 18$) and *hDAB2-KI* ($n = 20$) mice were intraperitoneally injected with anti-CD41 antibody (anti-CD41) daily for 2 days to induce ITP. Platelet number and bleeding time analyses were performed 24 h after final injection of anti-CD41. For analysis at the recovery phase (RP), *Rosa26*$^{fl/fl}$ ($n = 17$) and *hDAB2-KI* ($n = 13$) mice were injected with anti-CD41 daily for 2 days and experimentation was performed 72 h after final injection of anti-CD41. Platelet number was plotted and data represent the mean ± SEM (left of panel **a**). Unpaired two-sided Student's *t*-test was used for statistical analysis. A bleeding time assay was performed and the time when bleeding stopped was recorded. A bleeding time longer than 600 sec was set as 600 sec. Bleeding time was plotted and the horizontal lines represent the median of tail bleeding time (right of panel **a**). The percentage of mice with bleeding exceeding 600 sec in each group was indicated. The effect of *hDAB2-KI* on the bleeding time under thrombocytopenia and at RP was analyzed by the log-rank test (panel **b**). $p < 0.05$ was considered statistically significant. Exact *p* values for each group and Source data are provided as a Source Data file.

enhanced by adding ADP to the reaction (Fig. 6b, c). Clopidogrel (an antagonist of the ADP receptor $P2Y_{12}$) reversed the effect of hDab2 and increased the bleeding time of *hDAB2-KI* mice with thrombocytopenia ($p = 0.0025$), while having a minimal effect on mice with normal platelet counts (Fig. 6d, e). Augmentation of TxA_2-stimulated ADP/ATP release is therefore crucial for enhancing *hDAB2-KI* platelet aggregation at a low platelet concentration in vitro and reducing the bleeding time of *hDAB2-KI* mice with thrombocytopenia.

Consistent with the findings of *Rosa26*$^{fl/fl}$ and *hDAB2-KI* mice, analysis of platelets from patients with ITP ($n = 11$) revealed that the expression levels of platelet Dab2 were correlated with the intensity of U46619-stimulated ATP release ($r = 0.6930$, $p < 0.01$; Fig. 7a, Supplementary Table 2, and Supplementary Fig. 6). The bleeding score of ITP patients was inversely correlated with U46619-stimulated ATP release (Fig. 7b, $r = -0.6402$, $p < 0.05$) and platelet Dab2 expression (Fig. 7c, $r = -0.4601$, $p = 0.0772$). These data indicate that in thrombocytopenia, platelet Dab2 plays a key role in the control of U46619-stimulated ATP release and modulates the bleeding tendency in mice as well as in humans. The CD41 antibody-induced thrombocytopenia of *hDAB2-KI* mice is thereby a suitable model for addressing further how hDab2 enhances TxA_2 signaling leading to a reduced bleeding risk.

hDab2 regulates TxA_2-induced AKT-Ser473 phosphorylation and enhances TxA_2-induced first wave of ADP/ATP release

U46619 induces two waves of ADP/ATP release in platelets[30]. Lumi-aggregometer analysis showed that, at a platelet concentration of 1.8×10^8/ml, U46619 but not PAR4 peptide or collagen elicited two waves of ADP/ATP release (Fig. 8a). *hDAB2-KI* platelets displayed a 4.5-fold increase in the first wave of ATP release when compared to the *Rosa26*$^{fl/fl}$ platelets. The second wave of ATP release was not affected by hDab2. As a result, the total ATP release from *hDAB2-KI* platelets was 2-fold higher when compared to the *Rosa26*$^{fl/fl}$ platelets. In contrast, *hDAB2-KI* had no effect on PAR4 peptide- and collagen-stimulated ATP release (Fig. 8b). hDab2 thereby mainly regulates the signals leading to U46619-stimulated first wave of ADP/ATP release.

To understand how hDab2 enhances U46619- but not PAR4 peptide- and collagen-stimulated ADP/ATP release, *hDAB2-KI* platelets at the concentration of 1.8×10^8/ml were pretreated with the signal protein-specific inhibitors including the phospholipase C (PLC) inhibitor U73122, the phosphoinositide 3-kinase (PI3K) inhibitor wortmannin (Wort), the ADP receptor $P2Y_{12}$ antagonist Cangrelor (Can), and the phospholipase D1 (PLD1) inhibitor VU0155069 (VU1) followed by analysis of agonists-stimulated ADP/ATP release (Fig. 8c). A unique signaling pathway can be defined for the U46619-stimulated first wave of ADP/ATP release, which was PLC-dependent but PI3K-, $P2Y_{12}$- and PLD1-independent. In contrast, PAR4 peptide-stimulated ADP/ATP release was PLC-, and partially PI3K and $P2Y_{12}$-dependent, but PLD1-independent. Collagen-stimulated ADP/ATP release was PLC-, PI3K-, $P2Y_{12}$-, and PLD1-dependent.

AKT is a downstream effector of PLC and is associated with ADP/ATP release[31]. Platelet lysates were collected for Western blot analysis of AKT and AKT-related signaling proteins. At the initial phase of the first wave ADP/ATP release (15 sec after treatment), *Rosa26*$^{fl/fl}$ and *hDAB2-KI* platelets displayed similar levels of U46619-stimulated mTOR and PLD1 phosphorylation (Fig. 8d, e). AKT-Ser473 phosphorylation in *hDAB2-KI* platelets was augmented when compared to *Rosa26*$^{fl/fl}$ platelets. An immunoprecipitation assay further revealed that hDab2 interacted with AKT in U46619-stimulated but not resting *hDAB2-KI* platelets (Fig. 8f). This indicates that hDab2 expression potentiates hDab2-AKT interaction leading to AKT-Ser473 phosphorylation associated with the first wave of ADP/ATP release by U46619.

hDab2 is a PA-binding protein and recruits AKT to PA through an hDab2-AKT interaction

Interaction with membrane phospholipids is important for the function of AKT[32]. Previous studies demonstrated that hDab2 is a phospholipid-binding protein[33,34]. Whether or not the hDab2-AKT interaction recruits AKT to a specific phospholipid compartment leading to AKT activation was investigated. Profiling of the interaction between hDab2 and phospholipids was performed using membrane strips spotted with 15 types of lipids. GST-Dab2N which contains the N-terminal 234 amino acids of hDab2 protein interacted strongly with PA and PI4P, and moderately with PIP2 and PIP3 (Fig. 9a). GST-Dab2N only interacted with PA but not PI4P and PIP2 in the liposome binding assay, while the PI4P-binding protein GST-SidC-3C[35] and the PIP2-binding protein GST-PLC-δ1-PH[36] interacted with PI4P and PIP2, respectively (Fig. 9b). The equilibrium binding constant K_D for the hDab2-PA interaction was calculated to be 0.67 ± 0.24 nM by the surface plasmon resonance (SPR) assay (Fig. 9c). These data indicate that hDab2 is a PA-binding protein.

https://doi.org/10.1038/s41467-024-54093-5

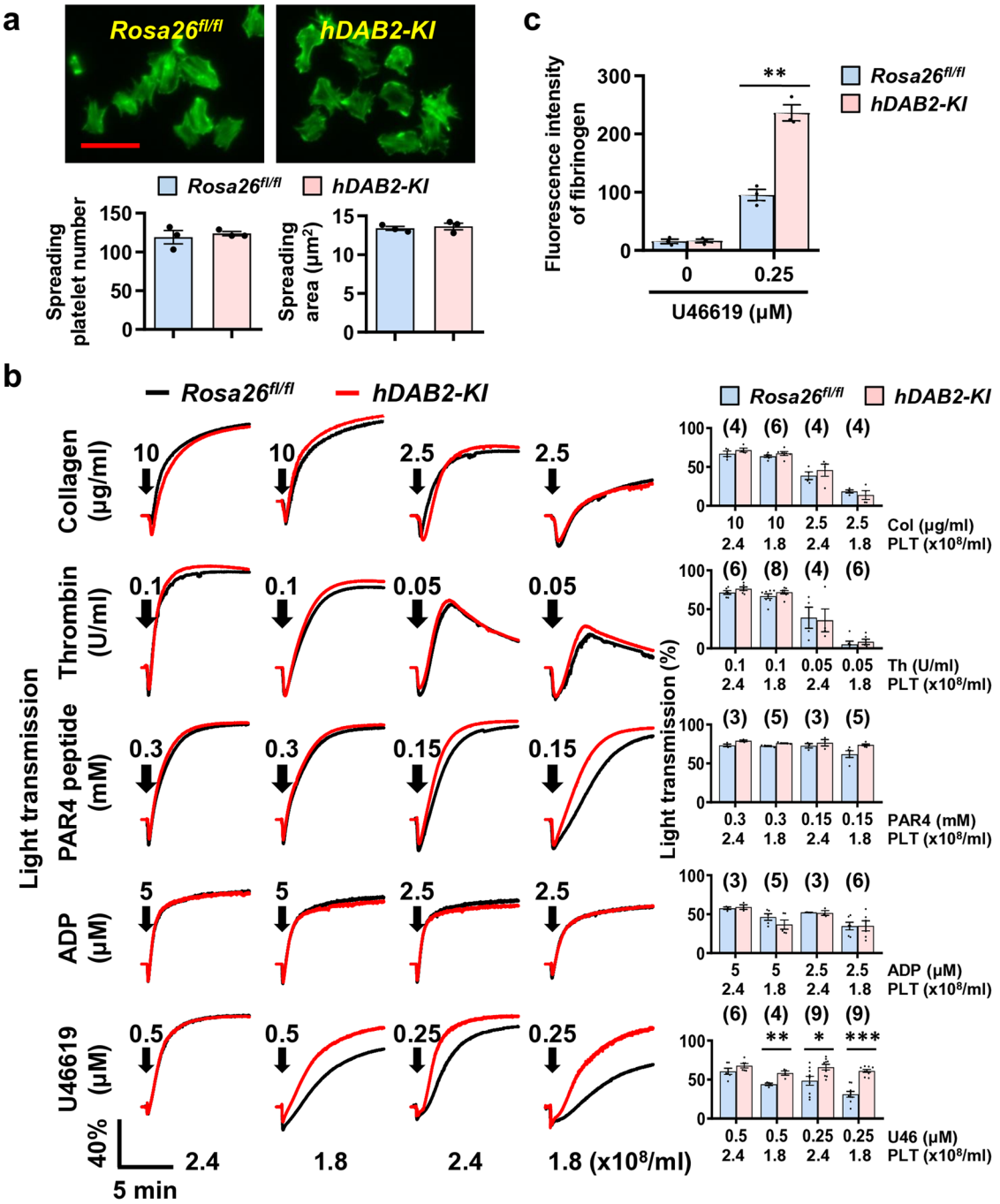

Fig. 4 | hDab2 selectively augments U46619-stimulated platelet activation at a lower platelet concentration of 1.8 × 10^8/ml in vitro. a Spreading of *Rosa26$^{fl/fl}$* and *hDAB2-KI* platelets on collagen was performed. The platelets were then labeled with FITC-conjugated phalloidin and recorded by fluorescence microscopy under a high power field (HPF) of 1000 X magnification. The images of spreading platelets are shown. The number and area of platelet spreading/HPF were determined. Data represent the mean ± SEM of 3 biological replicates each consisting of 3 random HPFs. scale bar = 10 μm. **b** Washed platelets were stimulated by the indicated soluble agonists and platelet aggregation was recorded by an AggRAMTM system (Helena Laboratories). Representative aggregation traces in response to collagen (Col), thrombin (Th), PAR4 peptide (PAR4), ADP, and U46619 (U46) at the indicated concentration of platelets and agonists are shown. Arrows indicate the point of adding the agonist into the reaction. The percentage of light transmission at the end of the aggregation assays was recorded. The number of biological replicates for stimulation of 2.4 x 10^8/ml and 1.8 × 10^8/ml platelets by high and low concentrations of agonists was 4, 6, 4, and 4, respectively for Col; was 6, 8, 4, and 6, respectively for Th; was 3, 5, 3, and 5, respectively for PAR4, was 3, 5, 3, and 6, respectively for ADP; was 6, 4, 9, and 9 for U46. Data represent the mean ± SEM. **c** Resting or U46619-stimulated (0.25 μM) platelets were incubated with Alexa Fluor 488-conjugated fibrinogen followed by flow cytometry analysis. Data represent the mean ± SEM of 3 biological replicates. Asterisks above the bars indicate statistically significant between groups based on unpaired two-sided Student's *t*-test (*$p < 0.05$, **$p < 0.01$, ***$p < 0.001$). Exact *p* values and Source Data are provided in Source Data file.

PA-binding sites contain at least one (R/K/H)(R/K/H) motif or one (R/K/H)x1-3(R/K/H) motif, where x is any residue[37]. GST-Dab2N contains two clusters of the PA consensus motif (Fig. 10a). To determine which cluster of the PA consensus motif is important for the Dab2-PA interaction, HA-tagged Dab2-20-45 and Dab2-167-186 peptides were synthesized. Dab2-20-45 peptide had a strong interaction with PA, while Dab2-167-186 peptide barely interacted with PA (Fig. 10b). To confirm the interaction of hDab2 and PA, GST-Dab2N mutants with

https://doi.org/10.1038/s41467-024-54093-5

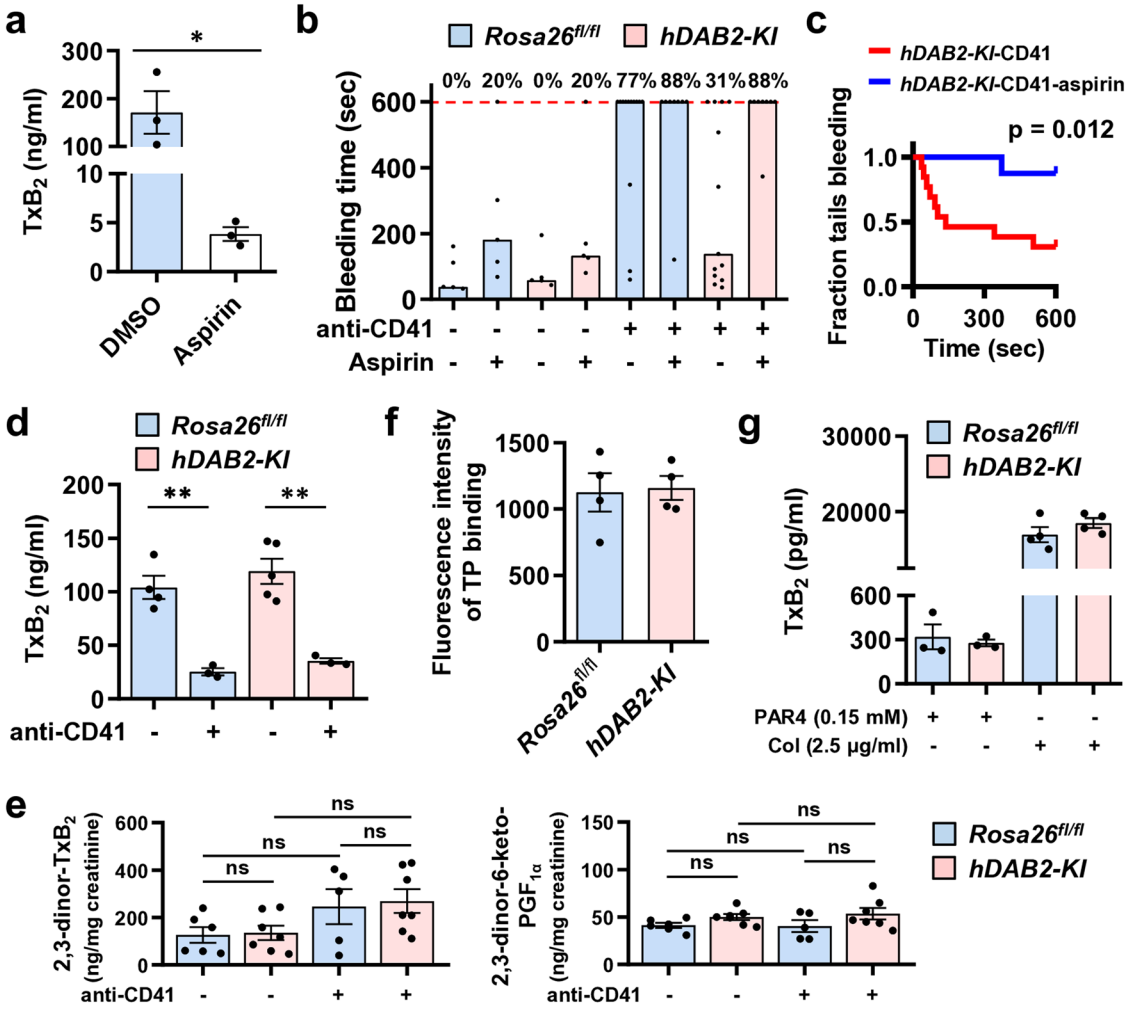

Fig. 5 | hDab2 regulates TxA_2 signaling leading to reduced bleeding time of *hDAB2-KI* mice with thrombocytopenia. a *Rosa26*$^{fl/fl}$ mice ($n = 3$ for each group) were treated daily for 7 days with solvent vehicle DMSO (2.5%) or low-dose aspirin (25 mg/kg) by oral gavage. Blood samples were collected for analysis of serum TxB_2 concentration. Data represent the mean ± SEM of 3 biological replicates each consisting of 3 technical replicates. **b** *Rosa26*$^{fl/fl}$ and *hDAB2-KI* mice were treated with vehicle control ($n = 5$), aspirin (25 mg/kg, $n = 5$), anti-CD41 antibody ($n = 13$) and anti-CD41 antibody with aspirin ($n = 8$), respectively. Bleeding time was recorded and the percentage of mice with bleeding time exceeding 600 sec of each group was indicated. A bleeding time longer than 600 sec was set as 600 sec. **c** The effect of low-dose aspirin on the bleeding time of *hDAB2-KI* mice under thrombocytopenia was analyzed by the log-rank test. $p < 0.05$ was considered statistically significant. **d** Blood samples of Rosa26$^{fl/fl}$ ($n = 4$ for vehicle control and $n = 3$ for anti-CD41 antibody) and *hDAB2-KI* ($n = 5$ for vehicle control and $n = 3$ for anti-CD41 antibody) mice were collected for analysis of the serum TxB_2 concentration. **e** 2,3-dinor-TxB_2 and 2,3-dinor-6-keto-$PGF_{1\alpha}$ present in the urine samples of *Rosa26*$^{fl/fl}$ ($n = 6$ for vehicle control and $n = 5$ for anti-CD41 antibody) and *hDAB2-KI* ($n = 7$ for vehicle control and anti-CD41 antibody) mice were determined by LC-MS/MRM and were normalized by the urinary level of creatinine. The two-sided Mann-Whitney U test was used for statistical analysis. ns, no significance. **f** Washed platelets were incubated with the FITC-conjugated anti-TP receptor antibody and analyzed by flow cytometry. Data represent the mean ± SEM of 4 biological replicates. **g** Supernatants from PAR4 peptide (PAR4, $n = 3$ biological replicates)- or collagen (Col, $n = 4$ biological replicates)-stimulated *Rosa26*$^{fl/fl}$ and *hDAB2-KI* platelets were collected for analysis of TxB_2 concentration. Asterisks above the bars in panel **a, d, f** and **g** indicate statistically significant between groups based on unpaired two-sided Student's *t*-test (*$p < 0.05$, **$p < 0.01$). Data represent the mean ± SEM. Exact *p* values and Source Data are provided in Source Data file.

substitution of lysine or arginine to alanine at the amino acid residues that potentially contribute to PA binding were generated. The recombinant proteins of hDab2 with K21A, K34A, R42A and K44A (GST-Dab2N-4M) or K25A, K26A, K28A, K29A and K30A (GST-Dab2N-5M) (Fig. 10c) were purified by Glutathione Sepharose 4B beads. The interaction of GST-Dab2N-4M or GST-Dab2N-5M with PA was decreased when compared with GST-Dab2N as determined by the liposome binding and protein lipid overlay (PLO) assays (Fig. 10d–f). This indicates that the lysine and arginine residues contribute to the binding of hDab2 to PA.

A PLO assay was performed to investigate whether or not AKT is recruited to PA through the Dab2-AKT interaction. Full-length hDab2 (GST-Dab2-FL) interacted with PA, similar to GST-Dab2N (Fig. 10g). Full-length AKT (His-AKT-FL) alone barely bound to PA (Fig. 10h). The AKT-PA interaction was enhanced when GST-Dab2-FL was present in the assay mixture. In contrast, GST-Dab2N was not able to enhance the AKT-PA interaction, consistent with the finding of a previous study[38] that showed that the putative AKT binding site is located at the C-terminal proline-rich domain of Dab2. This indicates that AKT is recruited to PA through a hDab2-AKT interaction.

Discussion

In this study, we revealed that platelet hDab2 reduces the bleeding time of mice with thrombocytopenia. hDab2 expression in platelets also inversely correlates with the bleeding tendency of ITP patients. Mechanistic investigation using the *hDAB2-KI* mouse model

https://doi.org/10.1038/s41467-024-54093-5

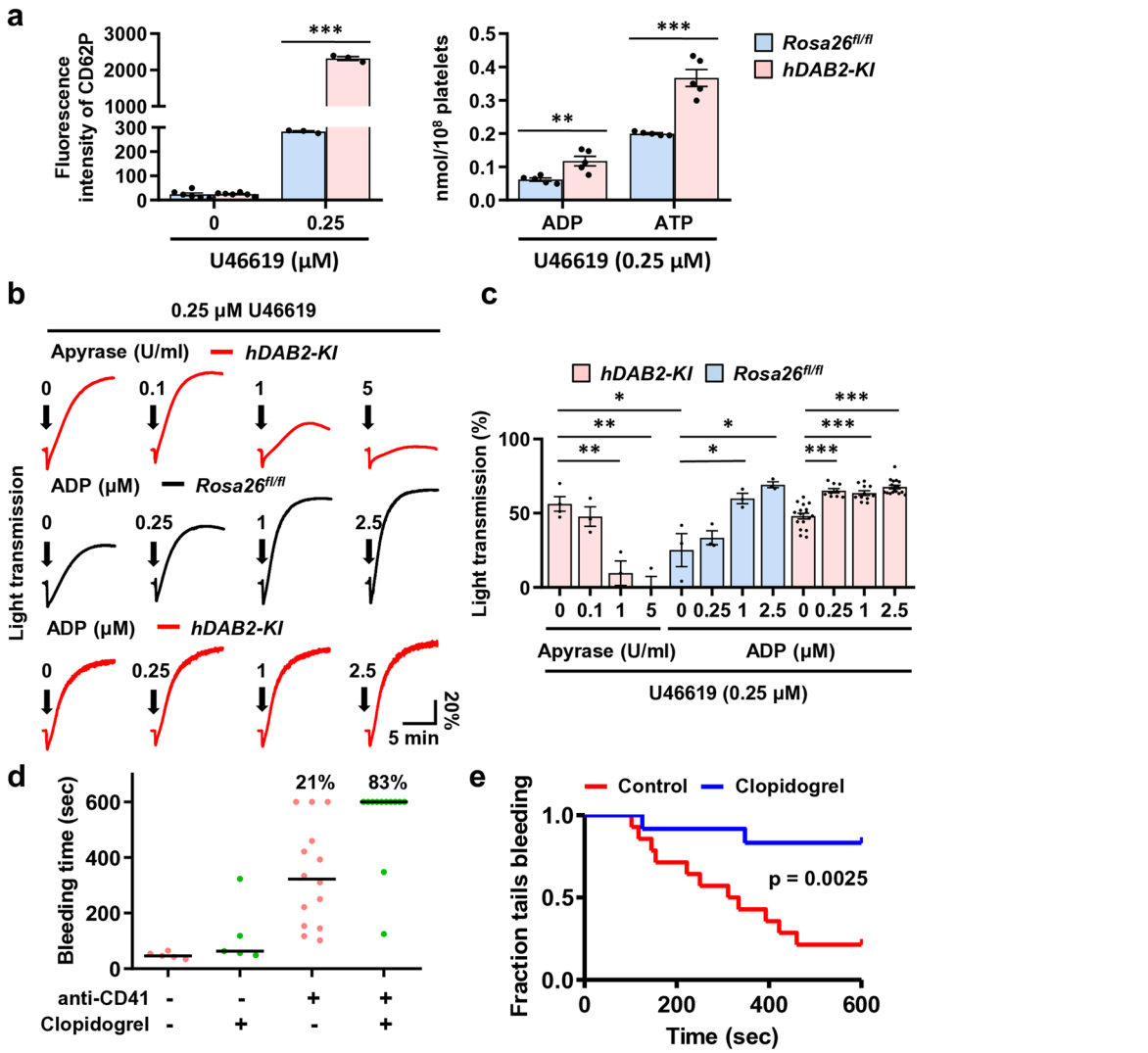

Fig. 6 | Augmentation of TxA_2-stimulated ADP/ATP release by hDab2 enhances platelet aggregation and reduces bleeding in mice with thrombocytopenia. **a** Resting ($n = 6$ biological replicates) and U46619-stimulated (0.25 μM, $n = 3$ biological replicates) platelets (1.8×10^8/ml) were incubated with PE-conjugated anti-CD62P antibody followed by flow cytometry analysis (left panel). Supernatants from U46619-stimulated (0.25 μM) platelets (1.8×10^8/ml) were collected. ADP and ATP release was analyzed and quantified using the GloMax 20/20 luminometer (right panel). Data represent the mean ± SEM of 5 biological replicates. **b**, **c** *hDAB2-KI* platelets (1.8×10^8/ml) were pre-incubated with the indicated concentrations of apyrase ($n = 4$, $n = 3$, $n = 3$ and $n = 3$ biological replicates for low to high concentration of apyrase) for 1 min and then stimulated with U46619 (0.25 μM). The *Rosa26*$^{fl/fl}$ ($n = 3$ biological replicates for each ADP concentration) and *hDAB2-KI* ($n = 17$, $n = 9$, $n = 11$ and $n = 17$ biological replicates for low to high concentration of ADP) platelets (1.8×10^8/ml) were stimulated with U46619 (0.25 μM) and the indicated concentrations of ADP simultaneously. Platelet aggregation was recorded by using the AggRAMTM system (Helena Laboratories). Representative traces for platelet aggregation are shown. Arrows indicate the point of adding agonists into the reaction. Data represent the mean ± SEM. Asterisks above the bars in panel **a** and **c** indicate statistically significant between groups based on unpaired two-sided Student's *t*-test (*$p < 0.05$, **$p < 0.01$, ***$p < .001$). **d**, **e** *hDAB2-KI* mice were treated with vehicle control ($n = 5$), clopidogrel (3 mg/kg, $n = 5$), anti-CD41 antibody ($n = 14$) and anti-CD41 antibody with clopidogrel ($n = 12$), respectively. A bleeding time assay was performed and the time when bleeding stopped was recorded. A bleeding time longer than 600 sec was set as 600 sec. Bleeding time was plotted and the horizontal lines represent the median of tail bleeding time (panel **d**). The percentage of mice with bleeding exceeding 600 sec in each group was indicated. The effect of clopidogrel on the bleeding time of *hDAB2-KI* mice under thrombocytopenia was analyzed by the log-rank test (panel **e**). $p < 0.05$ was considered statistically significant. Exact *p* values and Source Data are provided in Source Data file.

demonstrates that hDab2 expression has no effect on in vivo TxA_2 generation from platelets and PGI_2 biosynthesis from vascular cells. hDab2 acts as an adaptor protein to facilitate the formation of the PA-hDab2-AKT complex leading to an increase in U46619-stimulated AKT-Ser473 phosphorylation and the subsequent first wave of ADP/ATP release, which are crucial for the reduced bleeding of *hDAB2-KI* mice with thrombocytopenia. This is consistent with the findings that hDab2 expression in platelets was positively correlated with U46619-stimulated ATP release, which in turn inversely correlated with the bleeding tendency of ITP patients. This study facilitates our understanding of hDab2 function in platelets and provides mechanistic insight into the regulation of bleeding severity associated with thrombocytopenia.

At physiological concentration of platelets, both collagen and thrombin contribute significantly to platelet activation and cause an increase in TxA_2 biosynthesis and ADP release leading to platelet aggregation. TxA_2 is a weak platelet agonist. Its contribution to stimulating platelet aggregation is likely less than collagen and thrombin at normal platelet counts. The effect of platelet adhesion to collagen and thrombin generation are platelet density-dependent and are decreased in thrombocytopenia[39,40]. Despite the observations that the generation of TxB_2 ex vivo (serum) is relative to the platelet number in

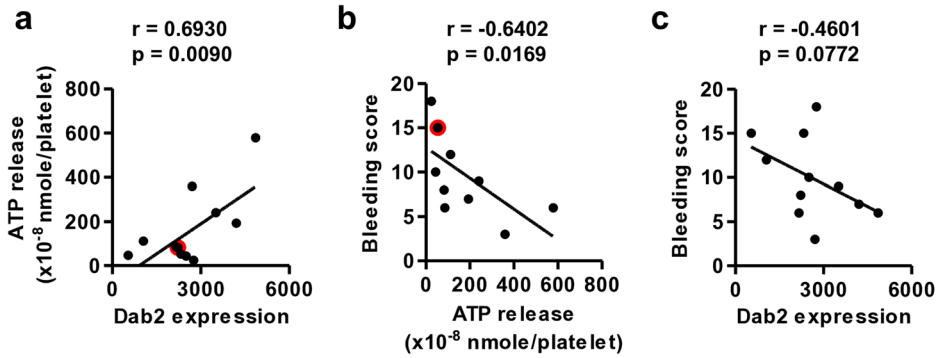

Fig. 7 | Correlation study of hDab2 expression in platelets, U46619-stimulated ATP release, and the bleeding score of ITP patients. a–c The peripheral blood from ITP patients ($n = 11$) was collected for analysis of platelet hDab2 expression and U46619-stimulated ATP release. The bleeding score was obtained at the initial stage of diagnosis. One-sided Pearson's correlation test was performed to evaluate the strength of correlation for the indicated variables. The strength of correlation was determined by the value of the correlation coefficient (r). The data dots that were close to each other were marked in red to indicate the presence of two data points in the plot. Source Data are provided in Source Data file.

mice and humans[29,41,42], in vivo TxA_2 generation was not altered and even slightly increased in the mice with thrombocytopenia. This is consistent with the finding that platelet cyclooxygenase activity in vivo is enhanced in chronic ITP[43]. TxA_2 signaling is postulated as a key pathway contributing to platelet activation and hemostasis in stopping bleeding under thrombocytopenic condition. Facilitating TxA_2 signaling and the subsequent ADP/ATP release by hDab2 thereby reduces the bleeding time of mice with thrombocytopenia with no effect on normal hemostasis. The importance of TxA_2 signaling in regulating hemostasis in thrombocytopenia is further supported by the findings that hDab2 expression in platelets positively correlated with the intensity of U46619-stimulated ATP release, which in turn elicited an inverse correlation with the bleeding tendency of ITP patients. In addition, U46619- but not thrombin- and collagen-stimulated ATP release from human platelet-rich plasma was highly variable among healthy individuals with a coefficient of variation equivalent of 88.9% at a low platelet concentration (0.1×10^8/ml) in vitro (Supplementary Table 3). This implies that the strength of TxA_2 signaling is variable among different individuals. The level of hDab2 expression in platelets is among the determining factors of the strength of TxA_2 signaling and the bleeding risk in thrombocytopenia. This is consistent with the notion that in addition to the platelet count, factors regulating platelet function contribute to the bleeding risk in thrombocytopenia[10,11]. Because hDab2 expression in platelets has no effect on TxA_2 generation and TP expression and does not cause thrombocytopenia or alter the normal vascular response to platelet activation, enhancing TxA_2 signaling and the subsequent ADP/ATP release by expression of Dab2 in platelets or by other mechanisms may provide a means to control bleeding associated with thrombocytopenia.

At the molecular level, Dab2 elicits multiple functions by interacting with cellular proteins and phospholipids, including sulfatide[44], integrin[12], and various cytoskeleton proteins such as myosin VI[45] and myosin heavy chain 9 (MYH9)[46]. We extend the list and report in this study that PA is an hDab2-binding partner by interacting with the positively charged N-terminus of hDab2. PA is a well-established second messenger with direct biological functions[47]. It is specifically recognized by diverse proteins and plays an important role in AKT activation/phosphorylation, cytoskeleton remodeling, and membrane dynamics[47]. With the estimated K_D of 0.67 nM for hDab2-PA binding and 0.6 mM for hDab2-sulfatide binding[44], hDab2 has a higher binding affinity with PA than with the sulfatide. It not only explains why the hDab2-PA interaction but not the hDab2-sulfatide interaction was observed in the PLO assay, but it also implies that the hDab2-PA interaction may elicit physiological functions that are worthy of further exploration.

Different mechanisms are related to the first and the second wave of TxA_2-stimulated ADP/ATP release[30,48,49]. The first wave of ADP/ATP release is regulated by a PI3K-independent manner[30]. The second wave of ADP/ATP release is PI3K-dependent and is regulated by Gi signaling initiated by the first wave of ADP/ATP release. We confirm and extend these findings showing that, at a lower platelet concentration, the first wave of ADP/ATP release was PLC- and Dab2-dependent, but PI3K-, $P2Y_{12}$-, and PLD1-independent. We further demonstrated that the underlying pathways leading to the first wave of ADP/ATP release by TxA_2 is distinctive from the signaling associated with PAR4 peptide- and collagen-stimulated ADP/ATP release. This may explain why hDab2 only augments U46619- but not PAR4 peptide- and collagen-stimulated platelet activation and ADP/ATP release at a lower in vitro platelet concentration.

hDab2 selectively enhances the first wave of U46619-stimulated ADP/ATP release by increasing AKT-Ser473 phosphorylation in a PI3K-independent manner. This is in contrast with the general understanding that AKT activation is PI3K-dependent. In the conventional view, AKT binds to PIP3 generated by PI3K through the PH domain[31]. PDK1 is recruited to PIP3 to phosphorylate AKT at Ser308[50]. PA-bound mTORC2 is crucial for the phosphorylation of AKT at Ser473 by mTORC2[51]. With PA and PIP3 having different spatial distribution on the cellular membrane, how PA-bound mTORC2 phosphorylates PIP3-bound AKT remains elusive. Because mTORC2 activity as revealed by its phosphorylation at Ser2481[52] is similar between *Rosa26*$^{fl/fl}$ and *hDAB2-KI* platelets, hDab2 regulates AKT activation/phosphorylation either at downstream of mTORC2 or through a mTORC2-independent manner. A model is proposed for AKT-Ser473 phosphorylation in which hDab2 binds to PA through a stretch of positively charged amino acids at the N-terminus and binds to AKT through the C-terminal proline-rich domain. The PA-bound hDab2 serves as a bridge for linking PIP3-bound AKT to PA to facilitate AKT-Ser473 phosphorylation by mTORC2. Alternatively, hDab2 may directly recruit cytoplasmic AKT to form PA-Dab2-AKT phospholipid-protein complex for Ser473 phosphorylation by mTORC2. This model is in contrast with the traditional view of PI3K-dependent AKT activation, but is consistent with the finding that AKT-Ser473 phosphorylation during the first wave of U46619-stimulated ADP/ATP release was PI3K-independent. In accord with this model, AKT is shown to translocate to the membrane and is activated in a PI3K-independent manner[53–55]. Phosphorylation of AKT at Tyr176 by the activated Cdc42-associated kinase 1, a protein tyrosine kinase that functions as a conveyer of signals from receptor tyrosine kinase and transmits cell proliferative signals via tyrosine phosphorylation of multiple downstream effectors[56,57], causes AKT translocation to PA leading to Ser473 phosphorylation and kinase activation[58].

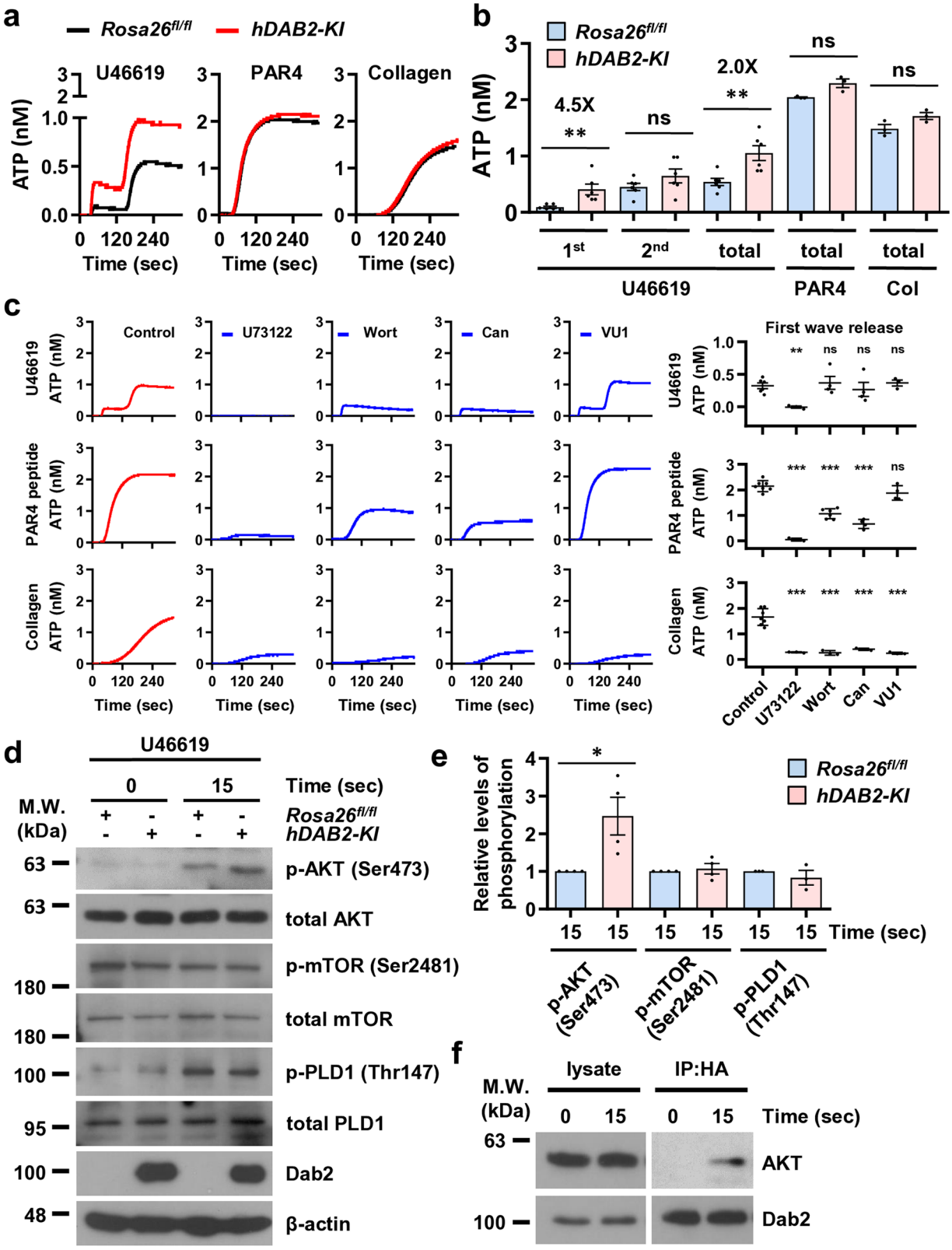

hDab2 most likely regulates AKT activation and the first wave of U46619-stimulated ADP/ATP release by a novel PI3K-independent mechanism involving the recruitment of AKT to PA by hDab2.

It is not clear whether or not the p59 isoform regulates TxA_2 signaling and the subsequent ADP/ATP release. The PA- and AKT-binding sites which are important for p82 function are present in p59, implying that an increase in p59 expression may also reduce the bleeding time of mice with thrombocytopenia. It cannot be ruled out that the deletion of 218 amino acid residues in p59 causes conformational change and affects the interaction of p59 with PA or AKT. Local change in the protein sequence, even with insertion of the 3 bps micro-exon[59], affects protein structure, subcellular localization, post-translational modification, enzymatic activity, and protein-protein interactions[60–64]. Generation of megakaryocyte

Fig. 8 | hDab2 regulates TxA_2-induced AKT-Ser473 phosphorylation and enhances TxA_2-induced first wave of ADP/ATP release. a, b ATP release of agonist-stimulated *Rosa26*$^{fl/fl}$ and *hDAB2-KI* platelets was detected by a Model 700 lumi-aggregometer (Chrono-Log). Representative traces for ATP release are shown. The amount of U46619-induced first wave (1st) and second wave (2nd) ATP release, and the maximal amount of ATP release (total) by U46619 ($n = 6$ biological replicates), PAR4 peptide (PAR4, $n = 3$ biological replicates) and collagen (Col, $n = 3$ biological replicates) were plotted. Data represent the mean ± SEM. **c** hDAB2-KI platelets were pre-incubated with 0.5 μM U73122, 500 nM wortmannin (Wort), 0.1 μM Cangrelor (Can) or 1.25 μM VU0155069 (VU1) and then stimulated with U46619 (0.25 μM), PAR4 peptide (0.15 mM) and collagen (2.5 μg/ml), respectively. ATP release was detected by a Model 700 lumi-aggregometer (Chrono-Log). Representative traces of ATP release are shown. Data represent the mean ± SEM. The number of biological replicates for control group and pretreatment of U73122, Wort, Can, and VU1 followed by U46619 stimulation was 6, 3, 4, 4, and 3, respectively; followed by PAR4 stimulation was 7, 3, 6, 4, and 4, respectively; and followed by collagen stimulation was 7, 3, 3, 3, and 3, respectively. **d, e** Washed platelets were stimulated by U46619 for 15 sec. Platelet lysates were analyzed by Western blot using the indicated antibodies. The relative level of phosphorylation was quantified by ImageJ software. Data represent the mean ± SEM of 4 biological replicates. Asterisks above the bars in panel **b, c** and **e** indicate statistically significant between groups based on unpaired two-sided Student's *t*-test (*$p < 0.05$, **$p < 0.01$, ***$p < 0.001$). ns, no significance. Exact *p* values and Source Data are provided in Source Data file. The representative Western blot images were derived from different experiments. **f** Lysates from resting or U46619-stimulated hDAB2-KI platelets were enriched by immunoprecipitation using the anti-HA antibody. The immunoprecipitated proteins were analyzed by Western blot using the anti-Dab2 and anti-AKT antibodies, respectively. Representative data from 4 biological replicates are shown.

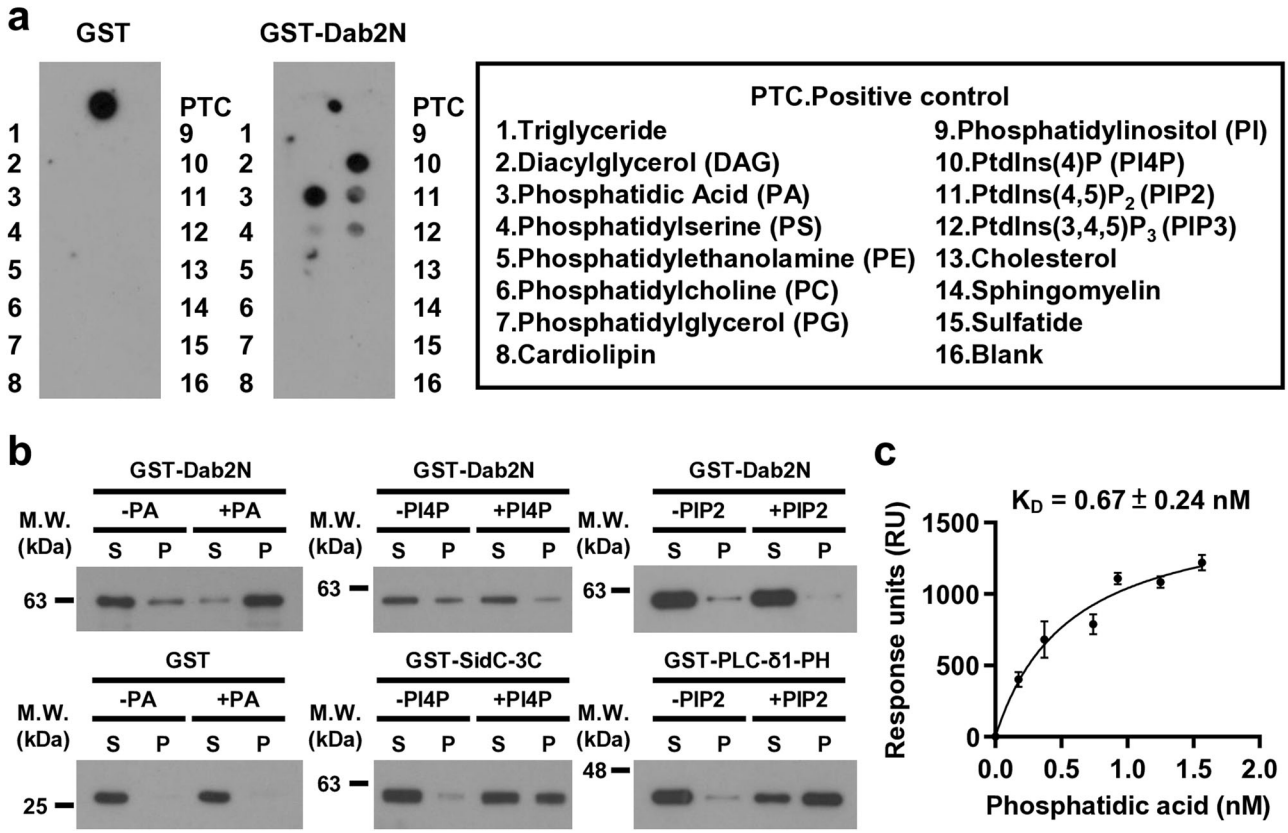

Fig. 9 | hDab2 is a PA-binding protein. a A membrane strip spotted with 15 types of lipids (100 pmol) was incubated with GST (8 nM, left panel) or GST-Dab2N (8 nM, right panel). The binding of recombinant proteins to lipids was immunodetected by using anti-GST antibody. GST or GST-Dab2N proteins were spotted directly on the nitrocellulose membrane as the positive control (PTC) for immunodetection. Representative data for at least 2 independent experiments are shown. **b** The indicated compositions of liposomes were incubated with GST-Dab2N, GST, GST-SidC-3C (a PI4P-binding protein) or GST-PLC-δ1-PH (a PIP2-binding protein), respectively. Proteins that were present in the supernatant (S) and the liposome pellet (P) fractions were analyzed by Western blotting using the anti-GST antibody. Representative data from at least 2 biological replicates are shown. **c** Interactions of PA with immobilized GST-Dab2N were analyzed by SPR. Response units were used to quantify the bound protein fraction at increasing PA concentrations. Data represent the mean ± SEM of 4 biological replicates for 0, 0.17, 0.37, 0.74, 0.93, and 1.56 nM PA and 3 biological replicates for 1.25 nM PA. The equilibrium dissociation constant (K_D) was calculated by using the built-in non-linear regression curve fit and the one-site binding model. Source Data are provided in Source Data file.

lineage-restricted p59 knock-in mice may facilitate defining p59 function in mice with thrombocytopenia.

In addition to mechanistic studies of mouse platelets, enrichment of hDab2-interacting proteins from human platelet lysates by immunoprecipitation (Supplementary Fig. 7) followed by proteomic analysis (Supplementary methods) revealed that the profiles of hDab2-interacting proteins were altered by treatment with U46619. This indicates that hDab2 underlies TxA_2 signaling in human platelets. KEGG pathway analysis further showed that hDab2-interacting proteins were mainly involved in the regulation of the actin cytoskeleton and platelet activation (Supplementary Table 4). For example, gelsolin participates in granule secretion[65]. When MYH9 is deficient, dense granule secretion stimulated by U46619- but not collagen- or high concentrations of thrombin was reduced[66]. This is consistent with the specific effect of hDab2 on TxA_2 signaling in mouse and human platelets in thrombocytopenia. The inverse correlation of hDab2

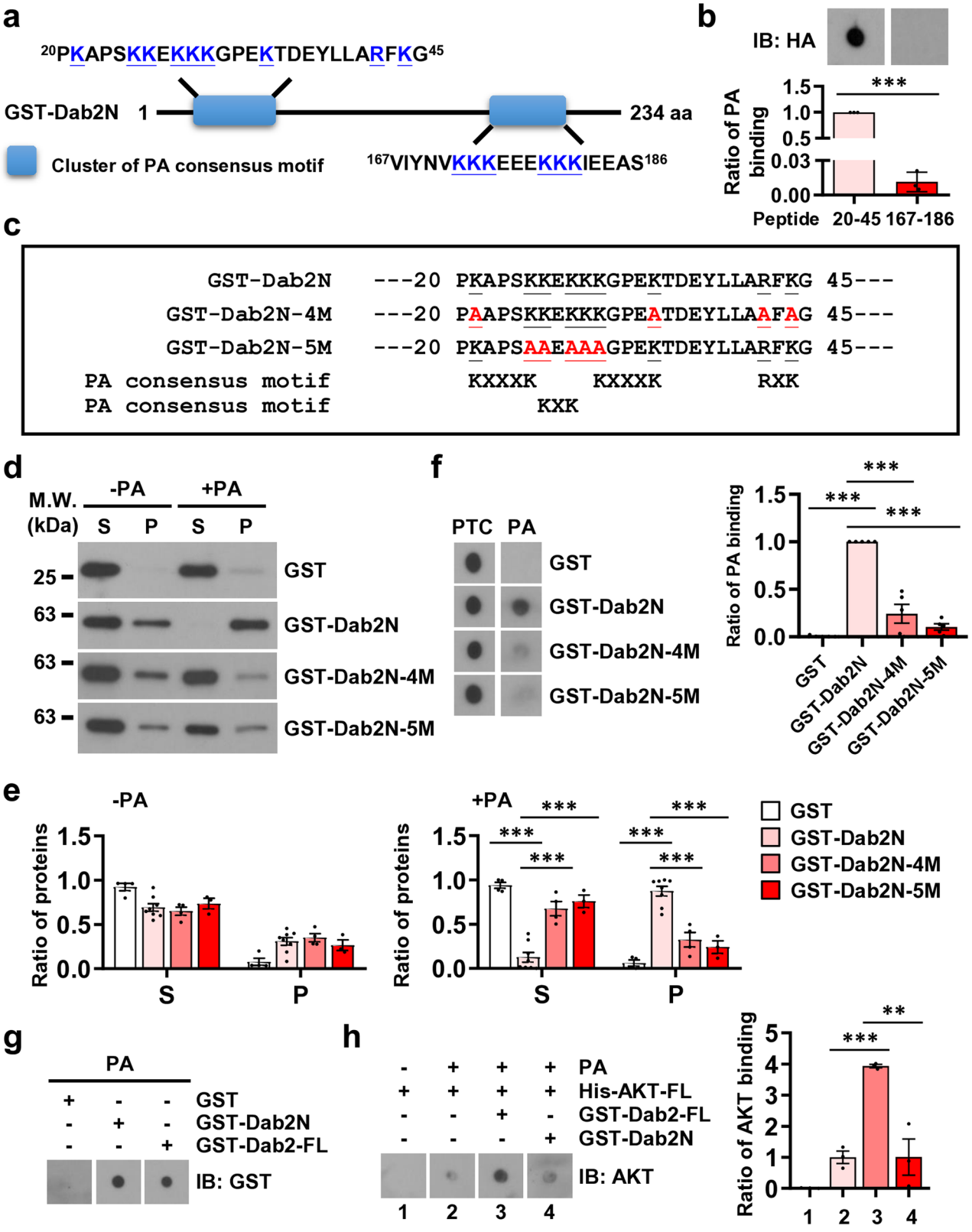

expression in platelets with the bleeding risk of ITP patients is not as robust as it is with the bleeding in the *hDAB2-KI* mice. Less statistical power in the analysis might be due to the small number of ITP patients enrolled in this study. Alternatively, the diverse genetic background and pathological causes among ITP patients and the complex signaling network for human platelet activation may contribute to the moderate inverse correlation of hDab2 expression in platelets with the bleeding risk. This warrants further increasing the number of ITP patients for investigation of hDab2 expression and function and its association with bleeding severity and TxA_2 signaling.

This study has several clinical implications. The bleeding assessment tools, based on physical examination or on patient's bleeding history supplemented by available reports rather than on platelet properties and function per se[67,68], is mainly used to assess the

Fig. 10 | AKT is recruited to PA through an hDab2-AKT interaction. a Illustration of the PA consensus binding motifs in GST-Dab2N. **b** The nitrocellulose membranes spotted with 1500 pmol PA were incubated with HA-Dab2-20-45 (20-45) and HA-Dab2-167-186 (167-186) peptides, respectively. The signal of PA binding in the 20-45 peptide group was arbitrarily set as 1. Data represent the mean ± SEM of 3 biological replicates. **c** The mutational sites of GST-Dab2-4M and GST-Dab2-5M. **d, e** The GST ($n = 4$ biological replicates), GST-Dab2N ($n = 8$ biological replicates), GST-Dab2-4M ($n = 4$ biological replicates) and GST-Dab2-5M ($n = 3$ biological replicates) proteins were incubated with 2 mM reconstituted liposomes in the absence or presence of PA. Proteins that were present in the supernatant (S) and the liposome pellet (P) fractions were analyzed by Western blotting using anti-GST antibody. Data represent the mean ± SEM. **f** The indicated proteins bound to the PA were immunodetected by using anti-GST antibody. The indicated recombinant proteins were spotted directly on nitrocellulose membrane as a positive control (PTC) for equal protein loading. The signal of binding to PA was quantified by ImageJ software. The signal of PA binding in the GST-Dab2N group was arbitrarily set as 1. Data represent the mean ± SEM of 5 biological replicates. **g** The binding of the indicated proteins to the PA was immunodetected by using anti-GST antibody. Representative data for 3 biological replicates are shown. **h** The nitrocellulose membrane was directly incubated with His-AKT-FL (lane 1), spotted with PA and incubated with AKT (lane 2), spotted with PA and incubated with AKT and GST-Dab2-FL (lane 3), or spotted with PA and incubated with AKT and GST-Dab2N (lane 4), respectively. The binding of AKT to the lipids was immunodetected by using anti-AKT antibody. Representative image for 3 biological replicates are shown. The mean signal in lane 2 was arbitrarily set as 1. Data represent the mean ± SEM of 3 biological replicates. Asterisks above the bars in panel **b**, **e**, **f** and **h** indicate statistically significant between groups based on unpaired two-sided Student's *t*-test (**$p < 0.01$, ***$p < 0.001$). Exact *p* values and Source Data are provided in Source Data file.

bleeding tendency of ITP patients in the clinical practice. The expression level of platelet hDab2 which is negatively correlated with the bleeding tendency of ITP patients may serve as a molecular biomarker to reflect platelet functions and supplement the bleeding scores for assessment of bleeding risk. The flow cytometric method we developed in this study provides an avenue to analyze platelet hDab2 expression and evaluate the bleeding tendency of ITP patients. We further define in this study that platelet hDab2 expression is positively correlated with TxA_2-stimulated ADP/ATP release which in turn inversely correlated with the bleeding tendency of ITP patients. Consistent with the clinical data, an increase in platelet hDab2 expression augments TxA_2-stimulated ADP/ATP release which subsequently reduces bleeding in mice with thrombocytopenia. The findings together imply that hDab2 and the TxA_2-signaling regulated by hDab2 are the potential targets for development of therapeutic regimens to reduce bleeding in ITP patients. Genetic approaches such as targeted gene therapy[69,70] can be developed to specifically increase hDab2 expression in megakaryocytes and platelets. Alternatively, molecular tools such as functional peptides[16,71] can be designed to enhance hDab2-regulated TxA_2-stimulated ADP/ATP release. These translational studies may further reinforce the clinical significance of our findings in this study.

The enhancing effects and the underlying mechanisms of hDab2 on reducing the bleeding time of mice with thrombocytopenia have been shown in this study. The level of hDab2 expression in platelets is linked to the release of ATP by U46619, which in turn elicits an inverse correlation with the bleeding tendency of ITP patients. The involvement of TxA_2 signaling and its regulation by hDab2 provides insight into the mechanisms associated with the bleeding risk of thrombocytopenia and additional options to assess bleeding risk and therapeutic strategies for ITP patients.

Methods

Generation of megakaryocyte lineage-restricted *hDAB2-KI* mice

Animal experiments were approved by the Institutional Animal Care and Use Committee (IACUC) with the Approval ID of CGU110-122 and were performed in accordance with the guidelines set by the IACUC. Mice were housed in filter top cages in Tecniplast units plus paper bedding within the Chang Gung University Animal Facility, with a 12 h light cycle from 7:00 am-7:00 pm, at temperature of 22 ± 1 °C and a relative humidity of 45%-55%.

The generation of *Rosa26*$^{fl/fl}$ mice was described in Fig. 1a–c. The megakaryocyte lineage-restricted *hDAB2-KI* mice were generated by cross-breeding *Rosa26*$^{fl/fl}$ mice with the *PF4-Cre* mice[26]. Both female and male mice at the age of eight- to twelve-week old were used in the study.

Genotyping of mouse strains

The following PCR primers were used for genotyping of newborn pups. P1 (5′-CTTGCTCTCCCAAAGTCGCT-3′) and P2 (5′-TCATGGAAATCT CCGAGGCG-3′), P3 (5′-GTGCTGGTTATTGTGCTGTC-3′) and P4 (5′-GGGCTGCTAAAGCGCATGCT-3′), and P5 (5′-CCCATACAGCACACCTT TTG-3′) and P6 (5′-TGCACAGTCAGCAGGTT-3′) were used for detection of wild-type *Rosa26* allele (+), fl allele, and *PF4-Cre* gene in the mouse genome with the PCR products corresponding to 447, 320, and 450 bps, respectively (Fig. 1a, c, d). The PCR condition for wild-type *Rosa26* (+) and fl allele was 1 cycle of 94 °C for 10 min, 20 cycles of 94 °C for 30 sec, gradually reduced 1 °C/sec/cycle from 65 to 55 °C for 30 sec and 72 °C for 1 min, 20 cycles of 94 °C for 30 sec, 55 °C for 30 sec and 72 °C for 1 min, and 1 cycle of 72 °C for 7 min. The PCR condition for the *PF4-Cre* gene was 1 cycle of 95 °C for 2 min, 40 cycles of 95 °C for 30 sec, 58 °C for 30 sec and 72 °C for 1 min, and 1 cycle of 65 °C for 5 min.

Bleeding time and rebleeding rate analysis

The mice were anesthetized by inhalation of isoflurane (NDC 60307-110-25, Piramal Critical Care, Bethlehem, PA, USA). The extremity of mouse tail was cut in a 0.5 cm length and was immediately immersed in 1X phosphate-buffered saline (PBS) prewarmed to 37 °C. Bleeding time was defined as the time required from excision to cessation of bleeding. The mice that rebled within 2 min after blood flow stop were defined as having the tendency of rebleeding.

Ferric chloride ($FeCl_3$)-induced mesenteric arteriole/venule thrombosis

Mouse was anesthetized with Zoletil (304801, Virbac, Nice, France):Rompun (Bayer Korea Ltd., Korea):saline (1:1:8) solution (140 µl/20 g body weight) by intraperitoneal injection. The fluorescent dye DiOC6 (318426, Sigma-Aldrich, St. Louis, USA, 1 mM in 1X PBS) was injected into mouse through the orbital venous plexus. Mesenteric arteriole/venule thrombosis was induced by 10% $FeCl_3$ (AF-12357, Alfa Aesar, UK)[72] and thrombus formation was video recorded using a fluorescence microscope for a maximal time interval of 40 min.

Transmission electron microscopy (TEM)

Platelet solution (2.4×10^8 platelets in 100 µl of Tyrode's buffer[73]) was fixed in 900 µl of 3% glutaraldehyde and 2% paraformaldehyde (PFA) at 4 °C overnight. The platelet pellet was collected, washed in 0.1 M phosphate buffer (pH 7.4), and incubated with 1% osmium tetroxide for 30 min at room temperature. After serial washing and dehydration with ethanol, the pellet was incubated with pure Epon overnight at 60 °C. Images of the ultrathin sections were obtained by using a transmission electron microscope (model Hitachi HT7800 TEM, Tokyo, Japan).

Animal model for thrombocytopenia and drug administration

Mice received daily intraperitoneal injection of anti-CD41 antibody[27] (133902, BioLegend, San Diego, CA, USA, MWReg30, 81.6 µg/kg/day for female mice and 122.4 µg/kg/day for male mice in 100 µl 1X PBS, pH 7.2) for 2 days to induce ITP. Experimentation was performed at 24 h

after final injection of the anti-CD41 antibody when the platelet count was below $5x10^8$/ml. Alternatively, experimentation at the recovery phase was performed at 72 h after the last injection of the anti-CD41 antibody. The platelet count at this phase was usually in the range of 5.2×10^8/ml to 13×10^8/ml.

To analyze the effects of low-dose aspirin on mice with thrombocytopenia, the mice were orally administered by oral gavage aspirin (A5376, Sigma-Aldrich, St. Louis, USA, 25 mg/kg) or its vehicle (2.5% DMSO) for 7 days[74]. At days 5 and 6, the mice also received intraperitoneal injections of the anti-CD41 antibody to induce ITP. Experimentation was performed 3 h after the last treatment of aspirin at day 7. To analyze the effects of clopidogrel (SANOFI, France) on mice with thrombocytopenia, the mice received daily intraperitoneal injection of the anti-CD41 antibody for 2 days. At day 2 and 2 h before bleeding time analysis at day 3, the mice also received clopidogrel (3 mg/kg) or its vehicle (0.9% NaCl)[75].

Washed platelets preparation

The mouse was anesthetized and blood was collected via cardiac puncture using a 25 gauge needle. Whole blood was mixed with sodium citrate (3.2%) and platelet-rich plasma (PRP) was collected by centrifugation at 200 g for 8 min. Platelets were obtained by washing PRP at 2,000 g for 6 min in the presence of 0.5 μM prostaglandin I_2 (18220, Cayman Chemical Co., Ann Arbor, Michigan, USA) and resuspended in Tyrode's buffer containing 1 mM $MgCl_2$ and 2 mM $CaCl_2$.

Platelet spreading and aggregation assay

Coverslips were coated with 10 μg/ml collagen (C3867, Sigma-Aldrich, St. Louis, USA) in 20 mM acetic acid at 4 °C overnight and were blocked for 30 min by 1% denatured BSA (A7906, Sigma-Aldrich, St. Louis, USA, at 70 °C for 1 h). The washed platelets (100 μl of 3×10^7 platelets/ml) were placed on collagen (C3867-1VL, Sigma-Aldrich, St. Louis, USA)-coated coverslips at 37 °C for 45 min. Nonadhered platelets were removed by washing twice using Tyrode's buffer. The adhered platelets were fixed with 4% PFA and permeabilized with 0.1% Triton X-100 following by staining with 100 nM acti-stain 488 phalloidin (PHDG1-A, Cytoskeleton Inc., Denver, CO, USA) at room temperature for 30 min. The number and area of spread platelets were quantified by ImageJ. For the platelet aggregation assay, washed platelets (2.4×10^8/ml or 1.8×10^8/ml) were incubated with agonists at 37 °C and analyzed using the AggRAM™ system (Helena Laboratories, Beaumont, Texas, USA).

Enrollment of ITP patients and blood collection

This study was approved by the Institutional Review Board of Taichung Veterans General Hospital (IRB No. CF23098C). Written informed consent was given by all patients or their legally authorized representatives, before inclusion in the study. A total of 11 patients with ITP that were undergoing treatment (3 males and 8 females, ages 7-54) were enrolled (Supplementary Table 2). The ISTH/SSC bleeding assessment tool was used to estimate the bleeding scores of the patients[67]. The bleeding risk was determined by the bleeding score according to the past medical history at initial diagnosis. Venous blood from recruited patients was collected into a BD Vacutainer Citrate tube (9 ml blood) and a BD Vacutainer K2 EDTA tube (1 ml blood). A Citrate tube was centrifuged at 670 *g* for 9 min to prepare PRP for the ATP release assay. The whole blood in the EDTA tube was subject to complete blood count analysis by Sysmex XN-350 (Sysmex Taiwan Co., Ltd., Taiwan) and Dab2 expression analysis by flow cytometry.

ADP/ATP release measurement

For end-point analysis of ADP/ATP release, the supernatants of agonist-stimulated platelets were collected for incubation with CellTiter-Glo reagent (G7570, Promega, Madison, WI, USA) and a potassium acetate/pyruvate kinase/PEP mixture at room temperature for 10 min. The luminescent signal was measured by using a GloMax 20/20 luminometer (Promega, Madison, WI, USA). For measurement of dynamic ATP release, the platelet suspension was mixed with the CellTiter-Glo reagent. The indicated agonists were added into the cuvette to start the reaction. ATP release was continuously monitored by using the Model 700 Lumi-aggregometer (Chrono-Log, Havertown, PA, USA).

Flow cytometry analysis

Resting or agonist-stimulated platelets ($6x10^7$/ml, 25 ml) were incubated with either 5 μl of PE-conjugated anti-CD62P antibody (0.05 μg/μl, 12-0628-82, eBioscience, San Diego, CA, USA), 5 μl of Alexa Fluor 488-conjugated fibrinogen (20 μg/μl, F13191, Invitrogen, Waltham, MA USA) or 5 μl of FITC-conjugated anti-TP receptor antibody (1 μg/μl, 10012559, Cayman Chemicals Co., Ann Arbor, Michigan, USA) for 20 min at room temperature in the dark. The reactions were stop by adding cold 1X PBS and the samples were analyzed within 30 min using an Accuri C6 Flow Cytometer with CFlow® Software (BD Biosciences, Franklin Lakes, NJ, USA).

For analysis of hDab2 expression in platelets, whole blood with EDTA anticoagulant was incubated with the 1-step Fix/Lyse Solution (00-5333, eBioscience, San Diego, CA, USA) for 15 min at room temperature for fixation of leukocytes and platelets and lysis of red blood cells. The pellets containing platelets and leukocytes were collected by centrifugation at 2700 *g* for 5 min and then washed twice with 1X PBS. After removal of the supernatants, the pellets were resuspended in 100 μl of 1X PBS and then permeabilized with 1 ml of 100% methanol for 30 min at 4 °C. After washing twice with 1X PBS, the pellets were resuspended with 3% BSA in 1X PBS. A portion of the platelet/leukocyte suspension was subject to flow cytometry analysis to estimate the platelet number in the suspension. The area in the forward scatter (FSC) vs side scatter (SSC) plot where platelets normally resided was gated. The number of particles in the area was counted for estimation of the platelet number in the sample. For immunofluorescent staining, the anti-Dab2 antibody [EP2297Y] (ab76253, Abcam, Boston, MA, USA) and the rabbit isotype IgG antibody were labeled with FlexAble FITC Plus Antibody Labeling Kit (KFA008) according to the manufacturer's instructions (Proteintech, Rosemont, IL, USA). Then platelets (2.5×10^5) were stained with the FITC-conjugated anti-Dab2 antibody and PE-conjugated anti-CD62P antibody (12-0628-82, eBioscience, San Diego, CA, USA) for 1 h at room temperature in the dark. Staining with the respective isotype control antibodies was performed simultaneously as a control of the background fluorescent signal. After 1 h of incubation, samples were washed twice with 1X PBS and resuspended with 100 μl of 1X PBS for analysis of hDab2 expression in platelets using an Accuri C6 Flow Cytometer with CFlow® Software (BD Biosciences, Franklin Lakes, NJ, USA). The particles in the P1 region of the FSC/SSC scatter plot with positive signal of PE-CD62P fluorescence (M1) were considered as platelets (M1 in P1, shown in Supplementary Fig. 6). Then the particles with positive signal of FITC-Dab2 fluorescence (M2, shown in Supplementary Fig. 6) in platelet fractions were selected and counted. The percent positive (%) and mean fluorescence for FITC-Dab2 was recorded. The relative levels of hDab2 expression in platelets was calculated by multiplying the values of percent positive (%) with the mean fluorescence.

Thromboxane B_2 (TxB_2) assay

Blood samples were obtained from the mouse retro-orbital plexus for analysis of TxB_2 concentration. After clotting of the whole blood at 37 °C for 1 h, serum was collected by centrifugation at 2000 *g* for 10 min for measurement of TxB_2. To determine TxB_2 production after in vitro platelet activation, 100 μl of 12 mM EDTA and 300 μM indomethacin were added into the agonist-stimulated washed platelet suspension to stop the reaction. The supernatants were collected by centrifugation (10,000 *g*) at 4 °C for 10 min followed by measurement of TxB_2. A Thromboxane B_2 ELISA Kit (501020, Cayman Chemicals Co.,

Ann Arbor, Michigan, USA) was used for the assay according to the manufacturer's instructions (Cayman Chemicals Co., Ann Arbor, Michigan, USA).

Mouse urine collection

Collection of 18 h mouse urine samples was performed as described previously with some modifications[76]. Briefly, mice at 6 h after the second intraperitoneal injection of anti-CD41 antibody or 1X PBS were individually placed in metabolic cages for 18 h with free access to tap water and food. Urine was captured into the urine collection tube outside the cage and was removed from the collection tube and transferred to the eppendorf containing sodium azide (final concentration of 1 mM) every 6 h. All urine samples from the same mouse were pooled, centrifuged at 1000 *g* for 10 min, aliquoted and stored at -80 °C (avoiding unnecessary freeze-thaw cycles) for further analysis.

LC-MS/MRM analysis for quantification of urinary 2,3-dinor-TxB_2 and 2,3-dinor-6-keto-$PGF_{1\alpha}$

For determination of urinary levels of 2,3-dinor-TxB_2 and 2,3-dinor-6-keto-$PGF_{1\alpha}$, 100 μl of mouse urine was spiked with 8 μl of an internal standard (IS) solution containing 2,3-dinor-6-keto-$PGF_{1\alpha}$-d9 (9000462, Cayman Chemicals Co., Ann Arbor, Michigan, USA) and 2,3-dinor-TxB_2-d9 (10009584, Cayman Chemicals Co., Ann Arbor, Michigan, USA) (32 pg/μl each). A liquid-liquid extraction technique was performed to enrich metabolites from the urine sample using 1 ml of ethyl acetate containing 0.13% acetic acid (v/v). After 10 min of shaking (1,500 rpm), samples were centrifuged (10,000 g) at 4 °C for 15 min. The organic layer (900 μl) was transferred to fresh tubes and dried by Speed Vac. The dry residue was reconstituted with 25 μl of 20% ethanol.

The reconstituted solution (5 μl) was injected into a Waters UPLC Acquity system (Waters, Milford, MA, USA) coupled to a triple quadrupole mass spectrometer QTRAP 6500+ (ABSciex, Framingham, Massachusetts, USA) for LC-MS/MRM analysis. Metabolites and the spiked deuterated IS were separated with an Acquity UPLC BEH C_{18} analytical column (1.0 × 100 mm, 1.7 μm) and eluted with buffer A (0.1% NH_4OH in water) and buffer B (pure ACN). Separation was performed with a liner gradient of 7% buffer B for 2 min, 7%-12% buffer B for 12 min, 12%-95% buffer B for 0.5 min, 95% buffer B for 1.5 min, 95%-7% buffer B for 1 min, and 7% buffer B for 3 min at a flow rate of 60 μl/min.

Data acquisition was carried out by multiple reaction monitoring (MRM) in the negative electrospray ion mode for all metabolites and deuterated IS. The operating parameters for mass spectrometer were set as follows: spray voltage: −4000 V, source temperature: 500 °C, curtain gas: 25 psi, ion source gas 1: 40 psi, and ion source gas 2: 50 psi. The quantifier transitions of Q1/Q3 pairs for 2,3-dinor-6-keto-$PGF_{1\alpha}$, 2,3-dinor-6-keto-$PGF_{1\alpha}$-d9, 2,3-dinor-TxB_2 and 2,3-dinor-TxB_2-d9 were *m/z* 341.3/205.3, 350.5/214.3, 341.3/155.3, and 350.5/164.3, respectively.

A calibration curve was established for quantification of 2,3-dinor-TxB_2 and 2,3-dinor-6-keto-$PGF_{1\alpha}$ in urine samples. Pooled mouse urine (100 μl) was spiked with 8 μl of 2-fold serial diluted deuterated IS (from 256 ng/ml to 1 ng/ml) followed by liquid-liquid extraction and LC-MS/MRM analysis as described above. The calibration curve for calculating the concentrations of 2,3-dinor-TxB_2 and 2,3-dinor-6-keto-$PGF_{1\alpha}$ was generated by plotting the peak area ratio between deuterated IS and analytes of interest *vs.* the concentration ratio between deuterated IS and analytes of interest using a linear regression model. Both 2,3-dinor-TxB_2 and 2,3-dinor-6-keto-$PGF_{1\alpha}$ levels were normalized against creatinine. Creatinine was measured by using the CREATININE liquicolor kit (10051, HUMAN Diagnostics Worldwide, Wiesbaden, Germany) according to the manufacturer's instructions.

Protein lipid overlay assay and liposome binding assay

For the PLO assay, nitrocellulose membranes spotted with lipids were incubated with the indicated proteins at 4 °C overnight. After washing, the membranes were incubated with the appropriate primary and secondary antibodies followed by detection using ECL-Plus reagents. For the liposome binding assay[77], the mixture of phosphatidylcholine (PC, 10009473, Cayman Chemicals Co., Ann Arbor, Michigan, USA) and PA (15082, Cayman Chemicals Co., Ann Arbor, Michigan, USA) (1.4:0.6) or PC alone were dried by a stream of nitrogen gas. After rehydration, liposomes were formed by sonication at 60 °C for 1 h. Liposome binding was performed by mixing the indicated proteins with liposomes at 23 °C for 10 min. The supernatant and liposome pellets were obtained by centrifugation at 9300 *g* for 10 min.

Surface plasmon resonance binding assay

SPR binding assays were performed on a TronViEWER system (PLASMONICTRON CO. LTD, Taiwan) according to the manufacturer's instructions. For ligand immobilization, the gold disk sensor was coated with a monolayer of 11-mercaptoundecanoic acid (11-MUA, 10 mM, 450561, Sigma-Aldrich, St. Louis, USA) via thiol groups overnight at room temperature and then washed three times with ethanol and double-distilled water (ddH_2O) sequentially. The gold disk sensor was incubated with 400 mM 1-ethyl-3-(3-dimethylaminopropyl) carbodiimide (EDC, E7750, Sigma-Aldrich, St. Louis, USA) and 100 mM N-hydroxy-succinimide (NHS, 130672, Sigma-Aldrich, St. Louis, USA) at room temperature for 10 min to activate the carboxylic group of 11-MUA. After washing three times with ethanol and ddH_2O sequentially, GST-Dab2N recombinant protein (0.1 pmol) in buffer C (20 mM Tris-HCl (pH 6.8) and 100 mM NaCl) was immobilized on the gold disk sensor surface by amine-coupling with the carboxylic group of 11-MUA for 40 min and then blocking with 0.3% bovine serum albumin in buffer C at room temperature for 20 min. All assays were performed according to the following procedure: equilibration with buffer C for 600 sec, PA association for 300 sec, and PA dissociation by buffer C for 300 sec. Regeneration of the GST-Dab2N recombinant proteins after the dissociation phase was carried out by washing the gold disk sensor with 20 mM NaOH for 300 sec. For kinetic binding experiments, various concentrations (0.17 to 1.56 nM) of PA were injected for 5 min at a flow rate of 40 μl/min onto the pre-immobilized GST-Dab2N gold disk sensor surface. Liposome concentrations of PA were calculated from particle numbers/ml of liposomes which were determined by using a NanoSight NS300 nanoparticle tracking instrument (Malvern Panalytical, Malvern, UK). The amount of bound PA with the GST-Dab2N protein was reported as response units (RU) for calculation of the equilibrium dissociation constant (K_D) using the built-in non-linear regression curve fit and the one-site binding model of GraphPad Prism 5 (GraphPad Software, Boston, MA, USA).

Statistical analysis

Statistical analysis of the bleeding time was determined by the log-rank test. The occlusion time for thrombus formation and the urinary levels of 2,3-dinor-TxB_2 and 2,3-dinor-6-keto-$PGF_{1\alpha}$ were analyzed by the two-sided Mann-Whitney U test between any two groups. Unpaired two-sided Student's *t*-test was used for all other analyses. The data represent the mean ± standard error of the mean (SEM). One-sided Pearson's correlation test was performed to evaluate the correlation between Dab2 expression, TxA_2-stimulated ATP release and the bleeding score using a GraphPad prism 5 software (GraphPad Software, Boston, MA, USA). The following equation shows the calculation of the Pearson's correlation coefficient, which is generally named as r:

$$r = \frac{N\sum xy - \sum x \sum y}{\sqrt{(N\sum x^2 + (\sum x)^2)(N\sum y^2 + (\sum y)^2)}} \quad (1)$$

where N is the number of samples, and x and y are two independent variables. The r was used to evaluate the strength of correlation. It was considered as moderate correlation when r was between 0.4 and 0.59, and as strong correlation when r was between 0.6 and 0.79[78].

A negative value of r indicates an inverse correlation of the variables. $p < 0.05$ was considered statistically significant.

Reporting summary

Further information on research design is available in the Nature Portfolio Reporting Summary linked to this article.

Data availability

All data are available in the main text or in the Supplementary Information. The mass spectrometry proteomic data generated in this study have been deposited in the ProteomeXchange Consortium with the dataset identifier PXD048490. Source data are provided with this paper. For original data and other information, please contact ctseng@mail.cgu.edu.tw. Source data are provided with this paper.

References

1. Tomaiuolo, M., Brass, L. F. & Stalker, T. J. Regulation of platelet activation and coagulation and its role in vascular injury and arterial thrombosis. *Interv. Cardiol. Clin.* **6**, 1–12 (2017).
2. Zhou, Y. et al. Mechanism of platelet activation and potential therapeutic effects of natural drugs. *Phytomedicine* **108**, 154463 (2023).
3. Theofilis, P. et al. Factors associated with platelet activation-recent pharmaceutical approaches. *Int J. Mol. Sci.* **23**, 3301 (2022).
4. Offermanns, S. Activation of platelet function through G protein-coupled receptors. *Circ. Res.* **99**, 1293–1304 (2006).
5. Lebas, H., Yahiaoui, K., Martos, R. & Boulaftali, Y. Platelets are at the nexus of vascular diseases. *Front. Cardiovasc. Med.* **6**, 132 (2019).
6. Bleeker, J. S. & Hogan, W. J. Thrombocytosis: diagnostic evaluation, thrombotic risk stratification, and risk-based management strategies. *Thrombosis* **2011**, 536062 (2011).
7. Jurk, K. & Shiravand, Y. Platelet phenotyping and function testing in thrombocytopenia. *J. Clin. Med.* **10**, 1114 (2021).
8. Scridon, A. Platelets and their role in hemostasis and thrombosis-from physiology to pathophysiology and therapeutic implications. *Int. J. Mol. Sci.* **23**, 12772 (2022).
9. Chen, Q. et al. Comparative study between two bleeding grading systems of immune thrombocytopenia purpura. *Hematology* **26**, 769–774 (2021).
10. Frelinger, A. L. et al. Platelet function tests, independent of platelet count, are associated with bleeding severity in ITP. *Blood* **126**, 873–879 (2015).
11. Frelinger, A. L. 3rd et al. Platelet function in ITP, independent of platelet count, is consistent over time and is associated with both current and subsequent bleeding severity. *Thromb. Haemost.* **118**, 143–151 (2018).
12. Huang, C. L. et al. Disabled-2 is a negative regulator of integrin alpha(IIb)beta(3)-mediated fibrinogen adhesion and cell signaling. *J. Biol. Chem.* **279**, 42279–42289 (2004).
13. Huang, C. L. et al. Disabled-2 is a novel alphaIIb-integrin-binding protein that negatively regulates platelet-fibrinogen interactions and platelet aggregation. *J. Cell Sci.* **119**, 4420–4430 (2006).
14. Tsai, H. J. et al. Disabled-2 is required for efficient hemostasis and platelet activation by thrombin in mice. *Arterioscler. Thromb. Vasc. Biol.* **34**, 2404–2412 (2014).
15. Tsai, H. J. et al. Functional links between Disabled-2 Ser723 phosphorylation and thrombin signaling in human platelets. *J. Thromb. Haemost.* **15**, 2029–2044 (2017).
16. Tsai, H. J. et al. Integrin alphaIIbbeta3 outside-in signaling activates human platelets through serine 24 phosphorylation of Disabled-2. *Cell Biosci.* **11**, 32 (2021).
17. Tsai, H. J. & Tseng, C. P. The adaptor protein Disabled-2: new insights into platelet biology and integrin signaling. *Thromb. J.* **14**, 28 (2016).
18. Maurer, M. E. & Cooper, J. A. Endocytosis of megalin by visceral endoderm cells requires the Dab2 adaptor protein. *J. Cell Sci.* **118**, 5345–5355 (2005).
19. Cho, S. Y., Jeon, J. W., Lee, S. H. & Park, S. S. p67 isoform of mouse disabled 2 protein acts as a transcriptional activator during the differentiation of F9 cells. *Biochem. J.* **352**, 645–650 (2000).
20. Rowley, J. W. et al. Genome-wide RNA-seq analysis of human and mouse platelet transcriptomes. *Blood* **118**, e101–e111 (2011).
21. Welsh, J. D. et al. Disabled-2 modulates homotypic and heterotypic platelet interactions by binding to sulfatides. *Br. J. Haematol.* **154**, 122–133 (2011).
22. Xiao, S. et al. Structure, sulfatide binding properties, and inhibition of platelet aggregation by a disabled-2 protein-derived peptide. *J. Biol. Chem.* **287**, 37691–37702 (2012).
23. Song, W. et al. Structural, in silico, and functional analysis of a Disabled-2-derived peptide for recognition of sulfatides. *Sci. Rep.* **10**, 13520 (2020).
24. Friedrich, G. & Soriano, P. Promoter traps in embryonic stem cells: a genetic screen to identify and mutate developmental genes in mice. *Genes. Dev.* **5**, 1513–1523 (1991).
25. Zambrowicz, B. P. et al. Disruption of overlapping transcripts in the ROSA beta geo 26 gene trap strain leads to widespread expression of beta-galactosidase in mouse embryos and hematopoietic cells. *Proc. Natl Acad. Sci. USA* **94**, 3789–3794 (1997).
26. Tiedt, R., Schomber, T., Hao-Shen, H. & Skoda, R. C. Pf4-Cre transgenic mice allow the generation of lineage-restricted gene knockouts for studying megakaryocyte and platelet function in vivo. *Blood* **109**, 1503–1506 (2007).
27. Nieswandt, B., Bergmeier, W., Rackebrandt, K., Gessner, J. E. & Zirngibl, H. Identification of critical antigen-specific mechanisms in the development of immune thrombocytopenic purpura in mice. *Blood* **96**, 2520–2527 (2000).
28. Morowski, M. et al. Only severe thrombocytopenia results in bleeding and defective thrombus formation in mice. *Blood* **121**, 4938–4947 (2013).
29. Alessandrini, P., Avogaro, P., Bittolo Bon, G., Patrignani, P. & Patrono, C. Physiologic variables affecting thromboxane B2 production in human whole blood. *Thromb. Res.* **37**, 1–8 (1985).
30. Li, Z. et al. Two waves of platelet secretion induced by thromboxane A2 receptor and a critical role for phosphoinositide 3-kinases. *J. Biol. Chem.* **278**, 30725–30731 (2003).
31. Woulfe, D. S. Akt signaling in platelets and thrombosis. *Expert. Rev. Hematol.* **3**, 81–91 (2010).
32. Chan, T. O., Rittenhouse, S. E. & Tsichlis, P. N. AKT/PKB and other D3 phosphoinositide-regulated kinases: kinase activation by phosphoinositide-dependent phosphorylation. *Annu. Rev. Biochem.* **68**, 965–1014 (1999).
33. Alajlouni, R., Drahos, K. E., Finkielstein, C. V. & Capelluto, D. G. Lipid-mediated membrane binding properties of Disabled-2. *Biochim. Biophys. Acta* **1808**, 2734–2744 (2011).
34. Spudich, G. et al. Myosin VI targeting to clathrin-coated structures and dimerization is mediated by binding to Disabled-2 and PtdIns(4,5)P2. *Nat. Cell Biol.* **9**, 176–183 (2007).
35. Luo, X. et al. Structure of the legionella virulence factor, SidC reveals a unique PI(4)P-specific binding domain essential for its targeting to the bacterial phagosome. *PLoS. Pathog.* **11**, e1004965 (2015).
36. Varnai, P. et al. Inositol lipid binding and membrane localization of isolated pleckstrin homology (PH) domains. Studies on the PH domains of phospholipase C delta 1 and p130. *J. Biol. Chem.* **277**, 27412–27422 (2002).
37. Zhukovsky, M. A., Filograna, A., Luini, A., Corda, D. & Valente, C. Phosphatidic acid in membrane rearrangements. *Febs. Lett.* **593**, 2428–2451 (2019).

38. Koral, K. et al. Akt recruits Dab2 to albumin endocytosis in the proximal tubule. *Am. J. Physiol. Ren. Physiol.* **307**, F1380–F1389 (2014).
39. Monroe, D. M., Hoffman, M. & Roberts, H. R. Platelets and thrombin generation. *Arterioscler. Thromb. Vasc. Biol.* **22**, 1381–1389 (2002).
40. Kjalke, M. et al. High-dose factor VIIa increases initial thrombin generation and mediates faster platelet activation in thrombocytopenia-like conditions in a cell-based model system. *Br. J. Haematol.* **114**, 114–120 (2001).
41. Carter, A. J. & Hanley, S. P. The effect of platelet number and haematocrit on whole blood thromboxane synthesis. *Thromb. Haemost.* **53**, 225–227 (1985).
42. Petrucci, G. et al. Platelet thromboxane inhibition by low-dose aspirin in polycythemia vera: Ex vivo and in vivo measurements and in silico simulation. *Clin. Transl. Sci.* **15**, 2958–2970 (2022).
43. Rousson, D., Guichardant, M., Lagarde, M., Viala, J. J. & Dechavanne, M. Increased in vivo biosynthesis of prostacyclin and thromboxane A2 in chronic idiopathic thrombocytopenic purpura. *Br. J. Haematol.* **72**, 402–406 (1989).
44. Drahos, K. E., Welsh, J. D., Finkielstein, C. V. & Capelluto, D. G. Sulfatides partition disabled-2 in response to platelet activation. *PLoS One* **4**, e8007 (2009).
45. Morris, S. M. et al. Myosin VI binds to and localises with Dab2, potentially linking receptor-mediated endocytosis and the actin cytoskeleton. *Traffic* **3**, 331–341 (2002).
46. Hosaka, K. et al. Megalin and nonmuscle myosin heavy chain IIA interact with the adaptor protein Disabled-2 in proximal tubule cells. *Kidney Int* **75**, 1308–1315 (2009).
47. Zhou H., Huo Y., Yang N., Wei T. Phosphatidic acid: from biophysical properties to diverse functions. *FEBS J*, https://doi.org/10.1111/febs.16809 (2023).
48. Hu, M. et al. Platelet Shp2 negatively regulates thrombus stability under high shear stress. *J. Thromb. Haemost.* **17**, 220–231 (2019).
49. Zhang, Y. et al. Receptor-interacting protein kinase 3 promotes platelet activation and thrombosis. *Proc. Natl Acad. Sci. USA* **114**, 2964–2969 (2017).
50. Alessi, D. R. et al. Characterization of a 3-phosphoinositide-dependent protein kinase which phosphorylates and activates protein kinase Balpha. *Curr. Biol.* **7**, 261–269 (1997).
51. Toschi, A. et al. Regulation of mTORC1 and mTORC2 complex assembly by phosphatidic acid: competition with rapamycin. *Mol. Cell. Biol.* **29**, 1411–1420 (2009).
52. Copp, J., Manning, G. & Hunter, T. TORC-specific phosphorylation of mammalian target of rapamycin (mTOR): phospho-Ser2481 is a marker for intact mTOR signaling complex 2. *Cancer Res* **69**, 1821–1827 (2009).
53. Mahajan, K. & Mahajan, N. P. PI3K-independent AKT activation in cancers: a treasure trove for novel therapeutics. *J. Cell Physiol.* **227**, 3178–3184 (2012).
54. Badolia, R., Manne, B. K., Dangelmaier, C., Chernoff, J. & Kunapuli, S. P. Gq-mediated Akt translocation to the membrane: a novel PIP3-independent mechanism in platelets. *Blood* **125**, 175–184 (2015).
55. Brugge, J., Hung, M. C. & Mills, G. B. A new mutational AKTivation in the PI3K pathway. *Cancer Cell* **12**, 104–107 (2007).
56. Shen, F., Lin, Q., Gu, Y., Childress, C. & Yang, W. Activated Cdc42-associated kinase 1 is a component of EGF receptor signaling complex and regulates EGF receptor degradation. *Mol. Biol. Cell* **18**, 732–742 (2007).
57. Wang, A. et al. Small molecules targeting activated Cdc42-associated kinase 1 (ACK1/TNK2) for the treatment of cancers. *J. Med. Chem.* **64**, 16328–16348 (2021).
58. Mahajan, K. et al. Ack1 mediated AKT/PKB tyrosine 176 phosphorylation regulates its activation. *PLoS One* **5**, e9646 (2010).
59. Chang, L. W., Tseng, I. C., Wang, L. H. & Sun, Y. H. Isoform-specific functions of an evolutionarily conserved 3 bp micro-exon alternatively spliced from another exon in Drosophila homothorax gene. *Sci. Rep.* **10**, 12783 (2020).
60. Irimia, M. et al. A highly conserved program of neuronal microexons is misregulated in autistic brains. *Cell* **159**, 1511–1523 (2014).
61. Tsyba, L. et al. Alternative splicing affecting the SH3A domain controls the binding properties of intersectin 1 in neurons. *Biochem. Biophys. Res. Commun.* **372**, 929–934 (2008).
62. Lei, J. et al. Conformational stability and dynamics of the cancer-associated isoform Delta133p53beta are modulated by p53 peptides and p53-specific DNA. *FASEB J.* **33**, 4225–4235 (2019).
63. Liu, Q., Fang, L. & Wu, C. Alternative splicing and isoforms: from mechanisms to diseases. *Genes (Basel)* **13**, 401 (2022).
64. Naschberger, A., Baradaran, R., Rupp, B. & Carroni, M. The structure of neurofibromin isoform 2 reveals different functional states. *Nature* **599**, 315–319 (2021).
65. Paul, M., Golla, K. & Kim, H. Gelsolin modulates platelet dense granule secretion and hemostasis via the actin cytoskeleton. *Thromb. Haemost.* **123**, 219–230 (2023).
66. Leon, C. et al. Megakaryocyte-restricted MYH9 inactivation dramatically affects hemostasis while preserving platelet aggregation and secretion. *Blood* **110**, 3183–3191 (2007).
67. Rodeghiero, F. et al. ISTH/SSC bleeding assessment tool: a standardized questionnaire and a proposal for a new bleeding score for inherited bleeding disorders. *J. Thromb. Haemost.* **8**, 2063–2065 (2010).
68. Rodeghiero, F. et al. Standardization of bleeding assessment in immune thrombocytopenia: report from the International Working Group. *Blood* **121**, 2596–2606 (2013).
69. Woods, V. M. A. et al. Targeting transgenic proteins to alpha granules for platelet-directed gene therapy. *Mol. Ther. Nucleic Acids* **27**, 774–786 (2022).
70. Martinez-Navajas, G. et al. Lentiviral gene therapy reverts GPIX expression and phenotype in Bernard-Soulier syndrome type C. *Mol. Ther. Nucleic Acids* **33**, 75–92 (2023).
71. Wallis, S. et al. A peptide from the staphylococcal protein Efb binds P-selectin and inhibits the interaction of platelets with leukocytes. *J. Thromb. Haemost.* **20**, 729–741 (2022).
72. Polak, D., Talar, M., Watala, C. & Przygodzki, T. Intravital assessment of blood platelet function. A review of the methodological approaches with examples of studies of selected aspects of blood platelet function. *Int. J. Mol. Sci.* **21**, 8334 (2020).
73. Lee, H. Y. et al. Podoplanin promotes cancer-associated thrombosis and contributes to the unfavorable overall survival in an ectopic xenograft mouse model of oral cancer. *Biomed. J.* **43**, 146–162 (2020).
74. Rohwer, N. et al. Effects of chronic low-dose aspirin treatment on tumor prevention in three mouse models of intestinal tumorigenesis. *Cancer Med* **9**, 2535–2550 (2020).
75. Lee, H., Sturgeon, S. A., Mountford, J. K., Jackson, S. P. & Hamilton, J. R. Safety and efficacy of targeting platelet proteinase-activated receptors in combination with existing anti-platelet drugs as antithrombotics in mice. *Br. J. Pharmacol.* **166**, 2188–2197 (2012).
76. Kovalcikova, A. et al. The effects of sucrose on urine collection in metabolic cages. *Lab Anim.* **53**, 180–189 (2019).
77. Tseng, W. L. et al. Impaired thrombin generation in Reelin-deficient mice: a potential role of plasma Reelin in hemostasis. *J. Thromb. Haemost.* **12**, 2054–2064 (2014).
78. Liang, Y. et al. How effective is pulse arrival time for evaluating blood pressure? Challenges and recommendations from a study using the MIMIC database. *J. Clin. Med* **8**, 337 (2019).

Acknowledgements

The authors thank the technical services provided by the Transgenic Mouse Model Core Facility of the National Core Facility Program for Biotechnology, National Science and Technology Council, Taiwan, and

the Gene Knockout Mouse Core Laboratory of the National Taiwan University Center of Genomic Medicine for generating the *Rosa26*$^{fl/fl}$ and *hDAB2-KI* mice. We acknowledge the editorial help from Professor Arnold Stern (New York University Grossman School of Medicine) and the support of metabolic cages and the SPR instrument from Professor Hung-Yao Ho (Chang Gung University) and Dr. Chia-Chen Chang (Chang Gung University), respectively. This work was supported by the Chang Gung Medical Foundation (Grant Numbers CMRPD1M0071-2 (CPT), CMRPD1N0211-3 (CPT) and BMRP466 (CPT)), the National Science and Technology Council (Grant Number 112-2320-B-182-047-MY3 (CPT)), and the China Medical University Hospital (Grant Number CMU111-MF-40 (JCC), and CMU112-MF-42 (JCC)).

Author contributions

Conceptualization, H.J.T. and C.P.T.; data curation, H.J.T., Y.F.C., Y.J.H., J.D.W., and C.P.T.; data analysis, H.J.T., Y.F.C., Y.J.H., J.D.W., C.C.W., M.Y.H., J.C.C., D.P.C., and C.P.T.; development or design of the methodology, H.J.T., Y.F.C., Y.J.H., C.C.W., M.Y.H., and C.P.T.; writing-original draft preparation, H.J.T. and C.P.T.; writing-review and editing, H.J.T., Y.J.H., J.D.W., C.C.W., J.C.C., D.P.C., H.R.L., and C.P.T.; funding acquisition, J.C.C. and C.P.T. All authors read and approved the final manuscript.

Competing interests

The authors declare no competing interests.

Additional information

Supplementary information The online version contains supplementary material available at https://doi.org/10.1038/s41467-024-54093-5.

Correspondence and requests for materials should be addressed to Ching-Ping Tseng.

Peer review information *Nature Communications* thanks Paola Patrignani, and the other, anonymous, reviewer(s) for their contribution to the peer review of this work. A peer review file is available.

Reprints and permissions information is available at http://www.nature.com/reprints

Publisher's note Springer Nature remains neutral with regard to jurisdictional claims in published maps and institutional affiliations.

Open Access This article is licensed under a Creative Commons Attribution-NonCommercial-NoDerivatives 4.0 International License, which permits any non-commercial use, sharing, distribution and reproduction in any medium or format, as long as you give appropriate credit to the original author(s) and the source, provide a link to the Creative Commons licence, and indicate if you modified the licensed material. You do not have permission under this licence to share adapted material derived from this article or parts of it. The images or other third party material in this article are included in the article's Creative Commons licence, unless indicated otherwise in a credit line to the material. If material is not included in the article's Creative Commons licence and your intended use is not permitted by statutory regulation or exceeds the permitted use, you will need to obtain permission directly from the copyright holder. To view a copy of this licence, visit http://creativecommons.org/licenses/by-nc-nd/4.0/.

© The Author(s) 2024